Research Square

Preprints are preliminary reports that have not undergone peer review.
They should not be considered conclusive, used to inform clinical practice,
or referenced by the media as validated information.

SoFIC Orchestrates Physical Barriers and Metabolic Homeostasis to Counter Phage Infection

Qun Jie
Tianjin University
Boxuan Yin
Tianjin University
Siyu Guo
Tianjin University
Sicheng Zhang
Tianjin University
Yong Li
Tianjin University
Lilin Zhang
Tianjin University
Deping Hua
Tianjin University
Xubin Fu
Ringpu Biotech lim. Co
Jinhai Huang
jinhaih@tju.edu.cn

Tianjin University

Article

Keywords: SoFIC, phage, E.coli, defense system, fimbriae biofilms

Posted Date: October 26th, 2026

DOI: https://doi.org/10.21203/rs.3.rs-11474419/v1

License: This work is licensed under a Creative Commons Attribution 4.0 International License.
Read Full License

Additional Declarations: No competing interests reported.

SoFIC Orchestrates Physical Barriers and Metabolic Homeostasis to Counter Phage Infection

Qun Jie[1,#], Boxuan Yin[1,#], Siyu Guo[1,#], Sicheng Zhang[1],Yong Li [1], Lilin Zhang[1], Deping Hua[1], Xubin Fu[2], Jinhai Huang[1,*]

1. School of Life Sciences, Tianjin University, Tianjin, 300072, China.
2. Ringpu Biotech lim. Co., Tianjin, 300000, China.

# These authors contributed equally to this work.

*Corresponding author at School of Life Science, Tianjin University, Tianjin 300072, China.; Tel and Fax: 86-22-27403902; E-mail address: jinhaih@tju.edu.cn

Abstract

Bacteria have evolved numerous defense systems to counter persistent phage infections. In this study, we characterize SoFIC, a protein encoded by *E. coli E5 that* catalyzes various post-translational modifications and coordinates a multilayed antiviral defense system by reshaping extrabacterial barriers and intracellular metabolism. Our results show that SoFIC is widely distributed across multiple bacterial phyla (particularly Proteobacteria) and exhibits diverse domain architectures; nonetheless, all variants contain a conserved Fic catalytic motif essential for anti-phage activity. Using the native host *E. coli* E5 and its cognate short-tailed phage DE5 as a model, knockout and complementation experiments demonstrated that the anti-phage function of SoFIC requires an intact Fic catalytic motif. Extracellularly, SoFIC physically hinders initial phage adsorption by maintaining surface structures such as fimbriae and biofilms. Intracellularly, once phages breach this barrier, SoFIC specifically interacts with key host proteins involved in DNA homeostasis (HupA, SbmC), transcription elongation (NusB), nucleotide metabolism (PyrB), and oxidative stress defense (Bfr, MsrA), preventing the host cell from entering a metabolic state conductive to phage proliferation. Furthermore, SoFIC exhibits time-dependent functional interactions with multiple endogenous defense systems, including Septu I, RM III, PsyrTA and Retron VI, collectively enhancing host immunity. Taken together, this study establishes SoFIC as a central coordinator of both physical and physiological antiviral barriers, reveals an extracellular and intracellular dual-layer defense model, and positions SoFIC as a key node in the multilayered bacterial immune network. These findings provide a theoretical basis for understanding the defense mechanisms of Fic family proteins and offer fundamental insights for engineering phage-resistant bacterial chassis.

Keywords: SoFIC; phage; *E.coli;* defense system； fimbriae； biofilms

Introduction

The long-term co-evolution between bacteria and their viruses (bacteriophages) drives the diversification of anti-phage defense systems, representing a major driving force of microbial evolution[1]. To defend against abundant phage infections in the environment, bacteria have gradually assembled a diverse arsenal of defense mechanisms that confer partial or complete immunity to the host[2]. Leveraging high-throughput bioinformatics and biostatistics, researches have now discovered hundreds of such defense systems, revealing the diverse strategies and complex interaction networks underlying bacterial immunity[3, 4].

Analogous to the immune systems of higher animals and plants, bacterial immune systems employ a multilayered, redundant defense strategy[5] to protect both individual cells and populations from phage infection. These defenses operate through multiple lines of barriers, including physical barriers[6, 7], innate immunity[8-10], adaptive immunity[11, 12] , and quorum sensing[13, 14]. Different bacteria assemble and arrange these diverse defense systems in unique combinations, forming robust and specific anti-phage barriers that function at distinct stages of the phage infection cycle[15, 16]. During the adsorption stage, bacteria primarily block phage attachment by modifying receptors[17-19], regulating receptor expression[20], or physically shielding receptors with structures such as biofilms[7] and capsular polysaccharides[21, 22]. If adsorption succeeds, intracellular defenses are rapidly deployed. During phage DNA injection, the Kiwa system, activated at the membrane site of phage attachment, directly binds and inhibits incoming phage DNA, achieving a form of spatial synergistic defense[23]. During phage DNA replication, the classic innate immune system RM specifically recognizes and cleaves foreign phage DNA[24, 25] , whereas the adaptive CRISPR/Cas system acquires fragments of viral DNA to establish a "memory" and executes precise clearance upon reinfection[26-29]. Moreover, recently discovered defense systems such as Shedu directly cleave invading phage dsDNA to confer immune protection[30]; the DrmAB complex of the DISARM system binds to phage DNA and activates the system's nuclease activity, thereby degrading phage DNA[31]. If phages manage to escape these early defenses, bacteria initiate abortive infection mechanisms that induce cell death, thereby blocking phage dissemination and protecting the bacterial population to the greatest extent[32]. Multiple newly identified systems, including Lamassu[33], CBASS[34],

Thoeris[35], and Kongming[36], sense phage invasion signals or infection-induced metabolic disturbances, produce or release second messengers, and subsequently activate downstream effectors that precisely cripple core metabolic pathways, leading to cell death.

The SoFIC defense system is a recently identified anti-phage system discovered through systematic bioinformatic screening of genomic defense loci. It consists of a single Fic family protein, SoFic[3]. The core of Fic family proteins is a Fic domain harboring the signature HPF(P/R)DGNGR motif, which catalyzes various post-translational modifications, including AMPylation, phosphorylation, and phosphocholination[37, 38]. Early characterized members of this family, such as VopS from *Vibrio parahaemolyticus* and IbpA from *Histophilus somni*, act as bacterial effectors that disrupt host cell cytoskeleton and signal transduction via AMPylation[39, 40]. However, subsequent genomic surveys have revealed that Fic domain-containing proteins are also frequently encoded within bacterial defense loci, often adjacent to phage resistance genes, strongly suggesting a potential role in antiviral immunity[41, 42]. Despite this, the anti-phage mechanism of the SoFIC system remains unknown. To date, only one heterologous expression study has reported that SoFIC confers resistance to the long-tail phage T5[42], but the molecular details of how it recognizes phage infection and exerts protection are still unclear. Moreover, most current studies on bacterial defense systems rely on heterologous overexpression systems that strip away native regulatory networks and inter-system cooperation[2, 30, 42]. This approach may miss the true physiological functions of defense systems, especially those that act as global regulators or require synergy with other immune components. Recent evidence indicates that defense systems do not act in isolation; instead, they form complex interaction networks that collectively confer robust phage resistance[43]. Bacteria in nature rarely depend on a single defense mechanism but rather deploy multilayered defenses to counter diverse phage challenges[3]. Nevertheless, whether SoFIC participates in such defense networks, and whether its role is limited to a single catalytic activity or extends to actively coordinating broader cellular responses, remain unresolved.

Here，we took advantage of *Escherichia coli* E5, a natural host of the SoFIC defense system, together with its cognate short-tail phage vB_EcoP_DE5. Using an integrated approach that combines molecular biology, phage infection assays, transcriptomics, proteomics, and

transmission electron microscopy, we systematically uncovered how SoFIC reshapes *E. coli* metabolic regulation and elucidated a novel immune mechanism against phage infection. Our study established a dual-layer model in which the SoFIC defense system resists phages by maintaining the bacterial physical barrier and regulating intracellular metabolic homeostasis, confirming the necessity of an intact Fic catalytic motif. Furthermore, we position SoFIC as a key node in the multilayered bacterial immune network, where it exhibits time-dependent functional crosstalk with multiple endogenous defense systems to collectively enhance host immunity.

Results

SoFIC systems is a widely distributed bacterial defense system

Data from DefenseFinder [44]showed that among 22,818 complete prokaryotic genomes, the SoFIC defense system was detected in 2,261 genomes spanning 1,159 different species, accounting for 9.91% of the total, indicating that SoFIC is a broadly distributed anti-phage defense system (Figure 1A). To further explore the diversity and abundance of SoFIC defense systems, we combined SoFIC defense system sequences predicted by PADLOC[45] from *Escherichia coli* E5 and *Escherichia coli* H397 with 629 SoFIC sequences previously predicted by Millman et al.[42]from 539 bacteria and archaea. This generated a dataset comprising 632 SoFIC defense system protein sequences derived from 541 bacterial and archaeal species (Table S1). Amino acid sequence alignment and phylogenetic tree construction were performed on this dataset (Figure 1B). The results revealed that SoFIC defense systems are widely distributed across multiple bacterial phyla, including Proteobacteria, Fusobacteria, Cyanobacteria, Spirochaetes, and Bacteroidetes. Among these, the distribution was most prevalent in Proteobacteria, a phylum representative of Gram-negative bacteria, accounting for 68.39% of the total (Figure 1C). This finding suggests that the SoFIC system may constitute a core component of the proteobacterial immune repertoire and may have co-evolved with proteobacteria-specific physiological features such as outer membrane architecture, secretion systems, and lifestyle, thereby forming a more efficient defense network[37, 38]. We next further subdivided Proteobacteria, the most abundant phylum, and found that SoFIC defense systems

are widely distributed in the orders Campylobacterales (22.4%), Neisseriales (18.1%), Lysobacterales (17.8%), Rhizobiales (10.3%), Enterobacterales (6.8%), and Burkholderiales (4.9%). Further subdivision within Enterobacterales showed that SoFIC defense systems are most prevalent in the family Enterobacteriaceae (80%) and the genus Escherichia (65%) (Figure 1D).

Based on the above distribution characteristics, we systematically analyzed the SoFic protein sequences in the dataset to dissect the functional basis and evolutionary patterns of SoFIC defense systems. The size of SoFic proteins in the dataset ranged from 195 to 455 amino acids, indicating substantial variation (Figure 1E). Moreover, the phylogenetic tree reconstructed from SoFic amino acid sequences did not strictly cluster according to established bacterial phyla. Instead, SoFic sequences from the same bacterial phylum exhibited polyphyletic origins, suggesting a complex evolutionary history for SoFIC defense systems potentially driven by frequent horizontal gene transfer (HGT) or convergent evolution (Figure 1B). Quantitative analysis of the number of SoFIC defense systems per bacterial genome revealed a non-uniform distribution. The majority of bacterial genomes (84.1%) carried a single SoFIC defense system, a smaller fraction (15%) carried two, and only a very small fraction (0.9%) carried three copies (Figure 1F). This indicates that in most bacteria, a single copy of the SoFIC defense system is sufficient to provide defense. Under specific ecological conditions such as high phage pressure, the presence of two SoFIC systems may confer synergistic defensive advantages[46]. Although additional copies might provide benefits under certain conditions, they are maintained at low frequency likely due to fitness costs such as metabolic burden or autoimmunity risks[47-49]. Collectively, these analyses demonstrate that the SoFIC defense system is a novel bacterial defense system characterized by wide distribution, high sequence diversity, and a predominantly single-copy genomic organization.

SoFIC systems is composed of structurally diverse Fic family proteins

To further investigate the structural basis of the *Escherichia coli* SoFIC defense system, we performed domain prediction and three-dimensional structure modeling using AlphaFold3 on SoFic proteins from 13 E. coli strains of the genus Escherichia within our dataset (Table S1).

This revealed three types of SoFic proteins with distinct domain architectures. Among them, SoFic proteins from 11 strains, represented by *E. coli* SF-166, harbored a Fic_N domain, a Fic domain, and a SoFic-like_C domain. *E. coli* S10 also contained both a Fic_N domain and a Fic domain but lacked the SoFic-like_C domain. In contrast, SoFic proteins from *E. coli* H397 and the experimental strain *E. coli* E5 used in this study contained only the core Fic domain (Figure 2A and 2B). The Fic domain is the core catalytic region responsible for SoFic protein activity. In most Fic protein structures, the Fic domain engages in extensive intramolecular interactions with N-terminal, C-terminal, or other internal domains of the Fic protein. These diverse intramolecular interactions give rise to multiple molecular conformations, but their importance for Fic protein function remains largely unclear[50-52]. The structural differences among the three SoFic proteins with distinct domain architectures further illustrate the critical role of such inter-domain intramolecular interactions in shaping the structural diversity of SoFic proteins.

We next performed protein motif prediction on the three aforementioned SoFic proteins and identified a continuous highly conserved region of 37 amino acids within the Fic domain. As expected, we recognized the canonical FIC motif HPF(P/R)DGNGR at positions 16 to 24 of this conserved region in all three proteins (Figure 2C), consistent with previous studies[37, 53], confirming that Fic domains share a common core composed of a helical topology and a conformationally highly conserved FIC motif. Notably, although Fic family proteins differ in their cofactors and protein substrates, all Fic proteins catalyze the same enzymatic reaction. The catalytic residues are located within the FIC motif (Figure 2D), including a conserved histidine residue that activates the threonine, tyrosine, or serine residue of the protein substrate for nucleophilic attack, a conserved arginine residue that stabilizes the negative charge of the phosphate group through electrostatic interactions, and a conserved acidic aspartate residue responsible for coordinating Mg^{2+} binding (highlighted in red). Other conserved residues may play auxiliary roles in the catalytic process by maintaining the fixed conformation of the FIC motif (highlighted in blue, green, and yellow)[37].

SoFIC provides anti-phage immunity in a Fic motif-dependent manner

To evaluate the anti-phage capacity of the SoFIC defense system, we cloned the sofic gene from *E. coli* E5 into the pET-28a vector and overexpressed it in *E. coli* BL21(DE3) (Figure 3A). We then challenged the SoFIC-overexpressing strain with a panel of phages representing the three morphological types of the order Caudovirales, namely the long-tail phage T5, the short-tail phage T7, and the myophage vB_EcoM_PD205. The results showed that the SoFIC defense system conferred strong resistance against the long-tail phage T5, reducing phage titers approximately 1,000-fold compared to the empty vector control (Figure 3B and 3E). This trend is consistent with a previous report[42]. SoFIC also exhibited weak resistance against the short-tail phage T7, reducing titers by about 10-fold (Figure 3C and 3E). However, it showed no detectable resistance against the myophage vB_EcoM_PD205 (Figure 3D and 3E). These results indicate that the protective effect of SoFIC is phage-selective. To further validate the resistance of SoFIC against phage T5, we infected BL21(DE3) cells carrying either an empty vector or the SoFIC-expressing construct with T5 at different multiplicities of infection (MOIs). Under low MOI conditions (0.01), SoFIC effectively protected the host, significantly suppressing T5 proliferation and leading to a much higher bacterial survival rate compared to the empty vector control. Under high MOI conditions (1), however, phages were numerically dominant, and the SoFIC defense was breached, failing to protect bacteria from T5 infection (Figure 3F). Next, to verify the critical role of the conserved Fic motif in the SoFIC defense system, we generated single mutants (H264A, D268A, R272A) and a triple mutant (H264A/D268A/R272A) of the three key catalytic residues in SoFic. We then challenged these mutant-expressing strains with phage T5. The results showed that mutation of any of these key residues caused a nearly complete loss of T5 resistance, with phage titers becoming indistinguishable from those of the empty vector control (Figure 3B). This confirms that the highly conserved Fic motif and its key catalytic residues are essential for the anti-phage function of SoFic.

We further constructed a sofic knockout strain in the natural host *E. coli* E5 (*E. coli* E5Δ SoFIC) (Figure S1B) and evaluated the native anti-phage phenotype of SoFIC using its cognate short-tailed phage vB_EcoP_DE5 (hereafter referred to as DE5). One-step growth curve results showed that the complete infection cycle of phage DE5 was approximately 1 h (Figure 4A).

Based on this, we infected wild-type and *E. coli* E5ΔSoFIC strains with DE5 at low and high MOI (Figure 4B). At the end of the first infection cycle (1 h), under low MOI conditions (0.001 and 0.01), the titer of phage DE5 in E5ΔSoFIC was significantly higher than that in the wild-type strain. As infection proceeded to 3 h, progeny phages had completed multiple rounds of infection. At this time, under low MOI conditions, the proliferation titer of DE5 in E5ΔSoFIC was more than tenfold higher than that in the wild-type strain. Further determination of bacterial lysis rate revealed that E5ΔSoFIC was almost completely lysed, whereas the lysis rate of the wild-type strain was only approximately 71% (Figure 4D and 4E). In addition, we monitored the dynamic changes in optical density under different MOI conditions, and the results showed that E5ΔSoFIC was lysed more rapidly (Figure 4C), confirming that the SoFIC defense system confers defense against phage DE5, and that loss of SoFIC renders bacteria more susceptible to phage infection. When infection proceeded to 5 h, a dynamic equilibrium was reached between phages and hosts; at this point, phage titer entered a plateau, and the difference in DE5 titer between the SoFIC knockout and wild-type backgrounds was narrowed (Figure 4B). Under high MOI conditions (1 and 10), however, SoFIC could not effectively protect bacteria against DE5 infection (Figure 4B), exhibiting a multiplicity-dependent defense characteristic consistent with the results from the heterologous expression system (Figure 3F).

To confirm that the above phenotypes were indeed caused by sofic deletion, we constructed complemented strains *E. coli* E5ΔSoFIC-WT (complemented with wild-type SoFic) and catalytic residue mutant complemented strains (complemented with H264A, D268A, R272A, and H264A/D268A/R272A mutants) (Figure S1C-S1E). Under low MOI infection conditions, after complementation with wild-type SoFic, phage titers decreased to levels comparable to those of wild-type E5 (Figure 4B), and the bacterial lysis rate recovered to approximately 70% (Figure 4D and 4E). In contrast, complementation with any single catalytic residue mutant or the triple mutant resulted in phage titers and bacterial lysis rates that were not significantly different from those of E5ΔSoFIC, consistent with the loss of resistance observed in the heterologous overexpression system (Figure 3B-3E). These results further confirmed in the native host background that SoFIC confers resistance to phages, and that this function depends on an intact Fic catalytic motif.

SoFIC deficiency compromises host physiology and cell surface architecture

Because heterologous expression systems inevitably alter the native transcriptional regulatory environment of sofic and lack potential cofactors or synergistic defense elements present in the original genome, they cannot fully reflect the authentic function and regulatory mechanism of SoFIC in its native host (Figure S1A; Table S2). Therefore, we focused on *E. coli* E5 and its cognate short-tailed phage DE5 to systematically investigate its regulatory capacity and the molecular mechanisms underlying its defense function in the original genomic context.

Transcriptome sequencing revealed that knockout of the SoFIC defense system significantly reduced the overall gene expression level in *E. coli* E5 (Figure S2A), indicating that SoFIC not only functions in defense but also positively maintains the overall transcriptional activity of the bacterium. Compared with the wild-type strain, E5ΔSoFIC strain had 35 significantly upregulated genes and 372 significantly downregulated genes ($|\log FC| \geqslant 1$ and $FDR \leqslant 0.05$) (Figure S2B). GO and KEGG enrichment analyses of the differentially expressed genes revealed that genes associated with the cell periphery, membrane, plasma membrane, flagella, and cell motility were significantly downregulated in E5ΔSoFIC (Figure S2C); correspondingly, pathways related to flagellar assembly, bacterial chemotaxis, quorum sensing, two-component systems, and nitrogen metabolism were also significantly downregulated (Figure S2D). Growth curves showed that knockout of the SoFIC defense system slightly reduced bacterial metabolic activity. Complementation with wild-type SoFic partially restored the growth defect of E5ΔSoFIC. In contrast, complementation with the H264A, D268A, or R272A single mutants or the triple mutant failed to restore bacterial growth (Figure 5A), suggesting that Fic catalytic activity is involved in maintaining normal host growth and metabolic status. Swimming motility assays further confirmed that the swimming radius of E5ΔSoFIC was reduced by 31% compared with the wild type (Figure S2E and S2F). In addition, crystal violet staining showed that biofilm formation in E5ΔSoFIC was reduced by approximately 55% (Figure S2G and S2H).

To further visualize the effect of SoFIC knockout on bacterial surface morphology, we observed wild-type *E. coli* E5 and *E. coli* E5ΔSoFIC by negative-staining transmission electron microscopy (Figure 5B). The results showed that compared to the wild-type, E5ΔSoFIC exhibited a marked reduction in peritrichous fimbriae, with cells becoming rounder and smoother and fewer surface protrusions. Whole-genome sequencing analysis of *E. coli* E5 revealed that it carries the fim gene cluster encoding type I fimbriae, the csg gene cluster encoding Curli fimbriae, and multiple additional fimbria-related gene clusters such as pap, sfa, and ecp. After SoFIC deletion, most genes in these clusters showed a downregulated trend at the transcriptional level (Figure 5C), suggesting an important regulatory role of the SoFIC defense system in fimbrial synthesis. To examine whether these transcriptional changes were reflected at the protein level, we further performed DIA quantitative proteomics on wild-type E5 and E5ΔSoFIC. Upon SoFIC deletion, the abundance of multiple fimbria-related proteins was significantly reduced, including the site-specific recombinase FimB, which is involved in type I fimbrial phase variation [54], the Curli transcriptional regulator CsgD, and the channel protein CsgG required for outer membrane secretion of Curli subunits[55] (Figure 5D and 5E). The significant decrease in FimB expression suggests impaired regulation of type I fimbrial phase variation, whereas the reduced abundance of CsgD and CsgG indicates impaired curli transcriptional regulation and defective curli subunit secretion and assembly, respectively.

Complementation with wild-type SoFic in E5ΔSoFIC largely restored the cell surface fimbrial structures to wild-type levels. In contrast, complementation with the H264A/D268A/R272A triple mutant resulted in only partial restoration of fimbriae, with the cell surface remaining smoother than that of the wild type and showing markedly insufficient surface protrusions and fimbrial density (Figure 5B). These findings indicate that intact Fic catalytic activity is crucial for maintaining normal fimbrial structures. Although the triple mutant partially restored fimbrial morphology, it was insufficient to rebuild a complete physical surface barrier. Overall, SoFIC broadly affects host physiological status and cell surface-related processes in a manner dependent on an intact Fic catalytic motif.

SoFIC hinders phage adsorption via the bacterial physical barrier

Given the reduced fimbriae and biofilm formation in the *E. coli* E5ΔSoFIC strain, we hypothesized that the SoFIC blocks initial phage adsorption by maintaining the surface physical barrier. Adsorption assays at 37 °C showed that phage DE5 adsorbed more rapidly to the knockout strain, reaching 91.9% at 10 min versus 79.8% for the wild type. Similar results were obtained at 4 °C, excluding interference from DNA injection (Figure 5F). Thus, SoFIC indeed impedes phage adsorption. Given the critical role of the Fic catalytic motif in restoring fimbrial structures, we further measured the adsorption rate of phage DE5 on the complemented strains (Figure 5F) to examine whether restoration of fimbrial structures was accompanied by restoration of anti-adsorption function. At both 37°C and 4°C, complementation with wild-type SoFic restored the DE5 adsorption rate to a level close to that of wild-type E5. After complementation with the H264A or D268A single mutant, the DE5 adsorption rate failed to decrease to wild-type levels. In contrast, after complementation with the R272A single mutant or the H264A/D268A/R272A triple mutant, the adsorption rate was almost identical to that of the E5ΔSoFIC strain and significantly higher than that of the wild-type strain. These results indicate that, in the native host genetic background, the fimbria-mediated structural barrier governed by an intact Fic catalytic motif is closely associated with the anti-adsorption function of the SoFIC, with the R272 residue being particularly critical under the present experimental conditions.

Subsequently, we identified the host surface receptor required by phage DE5. DE5 shares 96% genome sequence identity with phage SU10 (genus Kuravirus[56]), which uses lipopolysaccharide (LPS) as its receptor[57]. Host range analysis revealed that DE5 cannot infect the rough E. coli BL21 strain lacking O antigen, nor the *E. coli* E5 ΔwaaL mutant (O antigen ligase knockout), confirming that O antigen is an essential receptor (Figure 5G). Serotype prediction using SerotypeFinder[58] classified *E. coli* E5 as O2/O50 (Figure 5H). Notably, after SoFIC deletion, most O-antigen synthesis-related genes[59] were not upregulated but instead showed an overall downward trend (Figure S2I). Therefore, the enhanced DE5 phage adsorption on E5ΔSoFIC cannot be explained by upregulated receptor synthesis genes, but is more consistent with a steric hindrance-based defense model. In the wild-type strain, the SoFIC participates in maintaining the integrity of bacterial surface physical barriers such as fimbriae

and biofilms, thereby sterically blocking phage adsorption to host surface receptors. In contrast, the defective native physical barrier of E5ΔSoFIC allows a greater number of phages to adsorb to host receptors, rendering the bacteria more susceptible to phage infection.

SoFIC Initiates Multi-Target Synergistic Intracellular Defense upon Phage Stimulation

Although SoFIC can hinder initial phage adsorption by maintaining the bacterial physical barrier, it remains unclear whether it also participates in intracellular defense after phages breach the barrier. To address this, we further compared the transcriptomic changes between wild-type E5 and E5ΔSoFIC at 3 h after infection with DE5 at low MOI (0.01). In the absence of phages, the overall transcriptional level of E5ΔSoFIC was downregulated, whereas after infection its overall expression increased (Figure 6A), suggesting that successful phage replication forces the bacterium to switch from a low-metabolic dormant state to a global stress response state. Compared with the wild-type strain, E5ΔSoFIC had 163 significantly upregulated genes and 162 significantly downregulated genes ($|\log FC| \geq 1$ and FDR ≤ 0.05) (Figure 6B). GO and KEGG enrichment analyses of the differentially expressed genes revealed that downregulated genes were enriched in pathways such as the TCA cycle, DNA replication, mismatch repair, ribosomal protein synthesis, and ABC transporters (Figure S3B and S3D), indicating severe impairment of host basal metabolism and biosynthetic capacity. In contrast, upregulated genes were enriched in DNA damage response, homologous recombination repair, and purine and multiple amino acid metabolic pathways (Figure S3A and S3C). Because the cells already lacked sufficient energy and raw materials to complete effective repair, this repair activation not only failed to restore host homeostasis but likely provided nucleotide precursors and hijackable recombination machinery for phage genome replication, ultimately promoting phage proliferation.

To dissect the molecular basis by which SoFIC influences the above intracellular metabolic changes, we purified N-terminally His-tagged E. coli E5 SoFic protein and identified host proteins that specifically interact with SoFic upon DE5 phage stimulation by pull-down (Figure S4). Mass spectrometry results showed that SoFic interacted with 12 host proteins, including the DNA-binding protein HU-α (HupA), the transcription antitermination protein

NusB, the DNA gyrase inhibitor SbmC, the aspartate carbamoyltransferase catalytic subunit PyrB, bacterioferritin Bfr, and peptide methionine sulfoxide reductase MsrA (Figure 6C and 6D). These specifically interacting proteins are directly involved in key processes such as DNA homeostasis, transcription elongation, nucleotide metabolism, and antioxidation, closely matching the pathways enriched among the significantly differentially expressed genes in the transcriptome. HupA participates in maintaining DNA compaction, replication, and mismatch repair [60, 61]. SbmC, as a key regulator of DNA topology, is essential for maintaining DNA replication fidelity and suppressing unnecessary DNA damage stress [62]. Loss of SoFic interaction with HupA and SbmC may explain the downregulation of DNA replication and mismatch repair and the aberrant activation of homologous recombination in E5ΔSoFIC. NusB regulates ribosomal RNA transcription[63]; PyrB participates in pyrimidine synthesis[64]; Bfr and MsrA are involved in iron homeostasis[65] and oxidative repair[66], respectively. Their dysfunction may lead to decreased ribosomal synthesis, pyrimidine metabolic disorders, and reactive oxygen species accumulation[67] . Therefore, we propose that the SoFIC defense system helps maintain normal host DNA replication, energy metabolism, and protein synthesis while limiting excessive nucleotide synthesis and resisting oxidative stress. This effectively prevents host cells from falling into a disordered state of metabolic collapse and aberrant homologous recombination activation, providing a favorable environment for intracellular multi-layered defense and thereby inhibiting phage proliferation without killing the host.

Transmission electron microscopy further visually confirmed the above inference (Figure 6E). At 50 min post-infection, most wild-type E5 cells still maintained an intact rod-shaped structure, with a few intracellular phage particles undergoing assembly, and relatively few free phages were observed in the entire field of view. In contrast, E5ΔSoFIC already showed obvious signs of lysis, loss of cell membrane integrity, and leakage of cytoplasm, with numerous fully assembled phage particles visible within cells and near cell debris. Under high magnification (60,000×), large numbers of structurally intact phages could be clearly observed inside E5ΔSoFIC cells. At 3 h post-infection, the field of view for E5ΔSoFIC contained far more lysed cells and released progeny phages than that of the wild type, and high-magnification images revealed numerous fully assembled phage particles within the cells. These results are

consistent with the significantly higher lysis rate and phage titer of E5ΔSoFIC at 3 h post-infection compared with the wild type (Figure 4B and Figure 4D), indicating that after SoFIC loss, the intracellular environment was remodeled into a "phage factory" highly efficient at producing progeny phages.

SoFIC time-dependently synergizes with endogenous defense systems to enhance anti-phage immunity

Recent studies have shown that bacterial anti-phage defense systems interact extensively and can significantly enhance resistance to specific phages[3, 43]. To investigate the relationship between SoFIC and other endogenous defense systems, we individually knocked out all components or key genes of other predicted defense systems in the E5ΔSoFIC background (Figure S1B). Because knocking out the Lmuc component of Lamassu_Fam severely affected bacterial growth and knocking out the RM I system caused homozygous lethality, we were unable to obtain the corresponding double-knockout strains. The remaining double-knockout strains grew normally and could be used for subsequent infection experiments (Figure 7A).

After infection with DE5 at low MOI (0.01), phage titers were measured at 1, 3, and 5 h, and EOP (Efficiency of Plating) was calculated relative to the proliferation titer of the wild-type background (Figure 7B). At 1 h (Figure 7C), ΔAbiE, ΔRetron VI, ΔRM III, and ΔThoeris I showed significantly higher phage titers than the wild type (EOP = 10.58, 11.73, 6.35, and 3.15, respectively), indicating strong immediate defense. ΔSoFIC had an EOP of 3.27, confirming its role in early defense. In contrast, ΔSanaTA, ΔSeptuI, ΔPsyrTA, and ΔMenshen were similar to the wild type (EOP = 0.87-0.92), suggesting limited early defense. Among double knockouts, ΔSoFICΔSeptuI, ΔSoFICΔRMIII, and ΔSoFICΔPsyrTA reached EOP values of 11.73, 11.92, and 6.54, respectively, significantly higher than the corresponding single knockouts, indicating functional additivity or synergy. ΔSoFICΔAbiE, ΔSoFICΔSanaTA, ΔSoFICΔThoerisI, and ΔSoFICΔMenshen showed no significant difference from single knockouts, suggesting no obvious synergy with SoFIC.

After multiple rounds of infection (3 h) (Figure 7C), all single-knockout strains had titers significantly higher than that of the wild type (EOP = 16.67-26.39), with ΔSoFIC at 16.67.

Among double knockouts, ΔSoFICΔRetronVI reached an EOP of 26.39, significantly higher than either single knockout (16.67 and 18.06), indicating synergy. However, no synergy was observed between them at 1 h, indicating that the synergy between SoFIC and RetronVI is time-dependent. Similarly, ΔSoFICΔSeptuI showed early synergy at 1 h but had a lower titer at 3 h (EOP = 18.06) than ΔSeptuI alone (EOP = 26.39), suggesting that this synergy is restricted to early infection and is also time-dependent. Meanwhile, the lysis rate measurements (Figure 7D and 7E) showed that the wild-type strain had only 71% lysis, whereas all single and double knockouts exceeded 99%, confirming that the integrity of the defense systems is critical for bacterial survival during the middle and late stages of phage infection. At 5 h, all titers plateaued and differences from the wild type narrowed (EOP = 1.33-2.11) (Figure 7C).

To dissect this phenomenon at the molecular level, we compared the transcriptional changes of other endogenous defense system genes in ΔSoFIC and wild-type E5 before and after phage infection by transcriptomics (Figure S2J). In the uninfected state, most defense system genes in ΔSoFIC were already compensatorily upregulated at the transcriptional level. However, this transcriptional compensation was insufficient to overcome the core defense defect caused by SoFIC loss, as ΔSoFIC still exhibited phage titers and lysis rates far higher than those of the wild type after infection. At 3 h post-infection, the transcriptional levels of defense system genes changed again, and the trends differed among different systems. This indicates that bacterial defense systems do not act independently but constitute a highly complex, dynamically interacting regulatory network. Phage infection can trigger extensive remodeling of this network, which may explain the temporal heterogeneity of SoFIC interactions with other endogenous defense systems. However, the specific regulatory relationships still require further verification.

Discussion

Traditionally, functional studies of bacterial anti-phage defense systems have relied heavily on heterologous overexpression, where defense system genes are cloned into model strains for high-level expression to assess phage resistance. While convenient and experimentally tractable, this approach strips away the native transcriptional regulatory context, often missing the core physiological functions of the defense systems[3, 68]. To address this

limitation, we directly used *Escherichia coli* E5, a natural host of the SoFIC defense system, along with its cognate short-tail phage DE5. By constructing in situ knockout and complementation strains, we systematically revealed the authentic function of SoFIC in its native context and the immune mechanism underlying its defense against phage infection. Unlike most known bacterial anti-phage systems that directly target phage nucleic acids or proteins, SoFIC achieves dual-layer defense through an extracellular barrier effect and intracellular metabolic regulation by remodeling host metabolism and surface structures (Figure 8). In addition, SoFIC exhibits time-dependent functional crosstalk with multiple endogenous defense systems, collectively enhancing bacterial immunity.

Outer defense layer. SoFIC limits initial DE5 adsorption by maintaining the integrity of surface structures such as fimbriae and biofilms. Transcriptome and DIA proteomics consistently showed that SoFIC knockout reduced transcription of fimbrial gene clusters (*fim*, *csg*) and significantly downregulated FimB, CsgD, and CsgG. Knockout of SoFIC caused the fimbriae of E. coli E5 to almost disappear, reduced biofilm formation capacity by approximately 55%, and significantly increased the adsorption rate of phage DE5. Wild-type SoFic complementation restored growth, fimbriae, and the adsorption barrier, whereas complementation with H264A, D268A, R272A, or the triple mutant failed to restore full anti-adsorption function, indicating that an intact Fic catalytic motif is required for fimbria-mediated defense. Notably, the host surface receptor for DE5 is the O-antigen, whereas O-antigen synthesis genes were downregulated in ΔSoFIC, indicating that enhanced adsorption is not due to receptor upregulation but is more consistent with a model of physical barrier loss. Thus, SoFIC establishes a non-specific defense strategy based on steric hindrance that is multiplicity-dependent. It is effective at low MOI but can be overcome at high MOI. Given that the general abundance of phages in natural environments is usually insufficient to produce extremely high MOI, the SoFIC-mediated physical barrier may constitute the first line of defense for bacteria against phage invasion.

Inner defense layer. When phages breach the barrier, SoFIC initiates intracellular defense. Transcriptomics showed that ΔSoFIC underwent metabolic collapse after infection, with suppression of the TCA cycle, DNA replication, mismatch repair, and ribosomal synthesis, but

aberrant activation of homologous recombination repair and nucleotide precursor synthesis. Because cells lacked sufficient energy and raw materials to complete repair, these repair resources could instead be hijacked by phages, promoting their genome replication and packaging. TEM confirmed that ΔSoFIC produced numerous intact phage particles by 50 min post-infection, becoming an efficient “phage factory”. In contrast, wild-type SoFic interacts with HupA, SbmC, NusB, PyrB, Bfr, and MsrA to maintain DNA topology, replication fidelity, transcription elongation, pyrimidine synthesis, and redox homeostasis, thereby preventing metabolic collapse. Unlike abortive infection systems such as CBASS and Thoeris, SoFIC allows host survival while inhibiting phage proliferation, a strategy suited to ecological conditions with moderate phage pressure where host survival benefits the population.

Another key finding is the time-dependent functional perturbation between SoFIC and other endogenous defense systems. Single- and double-knockout experiments revealed that SoFIC synergizes with Septu I, RM III, PsyrTA, and Retron VI in a time-dependent manner. SoFIC synergizes with SeptuI only in the early stage of infection, whereas its synergy with RetronVI occurs in the middle stage of infection. Transcriptomic analysis further indicated that SoFIC deficiency perturbs the transcriptional status of other defense systems. Phage infection triggers further dynamic changes at the transcriptional level, indicating that defense systems do not act independently but constitute a complex and dynamically interacting regulatory network. Although most defense system genes in E. coli E5ΔSoFIC are compensatorily upregulated, this is still insufficient to compensate for the core defense defect caused by SoFIC loss, suggesting that SoFIC may be a key node in maintaining the coordination of this defense network; however, the precise regulatory relationships require further verification.

Previously, Fic family proteins were thought to participate primarily in bacterial toxin activity, metabolic regulation, or cellular signal transduction through post-translational modifications such as AMPylation[37, 38]. However, the present work directly links Fic family proteins to anti-phage defense. We found that SoFic contain a conserved Fic catalytic motif, and three key catalytic residues (H264, D268, R272) are essential for its anti-phage activity of SoFIC(Figure 3B-3E). This functional shift suggests that the Fic domain may have been domesticated through distinct evolutionary mechanisms: as an effector, it is used to attack the

host; as a defense component, it is repurposed to remodel the bacterium's own metabolism and structural state. Nevertheless, we have not yet identified the direct modification substrates of SoFic. Whether the interaction partners identified by pull-down (HupA, SbmC, NusB, PyrB, Bfr, MsrA) are directly modified by SoFic, as well as the modification sites and functional consequences, remain to be addressed in future studies. In addition, this study has not yet elucidated the molecular mechanism underlying the defense selectivity of SoFIC against different phages. Based on our dual-layer defense model, however, several plausible explanations exist: (1) different phages may differ in their ability to penetrate the surface physical barrier[69]. T5, as a long-tail phage, has a long and flexible tail that may be more easily impeded by dense fimbrial and biofilm matrices[57]. Whereas T7, a short-tail phage, has a shorter and more rigid tail that may confer stronger penetration ability, allowing it to partially bypass the physical barrier[70]; (2) phages vary in their reliance on host metabolism. T5 heavily depends on host replication, nucleotide synthesis, and energy metabolism, making it more susceptible to SoFIC-mediated metabolic homeostasis, whereas T7 rapidly shuts down host metabolism or encodes its own metabolic enzymes, limiting SoFIC efficacy[71, 72]; (3) some phages may encode anti-defense proteins that inhibit SoFIC or its host interactions—a possibility requiring future genomic screening[36].

In conclusion, this study establishes a dual-layer anti-phage defense model for SoFIC, combining an external barrier effect and internal metabolic regulation. This work expands the functional diversity of Fic family proteins and reveals a non-abortive infection strategy based on global metabolic remodeling rather than cell death. The time-dependent functional crosstalk among defense systems offers new insights into the hierarchical architecture of the bacterial immune network. From an applied perspective, these findings provide a theoretical foundation for engineering "domesticated" phage-resistant bacterial chassis with controllable metabolic burden, with potential applications in phage therapy, industrial fermentation, and synthetic biology.

Materials and Methods

Bacterial strains, plasmids, and culture conditions

All bacterial strains, plasmids, and primers used in this study were listed in Table S3-S5 respectively. *Escherichia coli* strains were routinely cultured in Luria-Bertani (LB) broth or on LB agar plates at 37°C with shaking. The whole genome sequence of phage DE5 and its *E coli* host E5 strain were sequenced and deposited in GenBank (Accession number: MW741821.1[56] and JBYDFN000000000 respectively). When necessary, antibiotics were added to the medium to maintain plasmid stability at the following concentrations: ampicillin (100 μg/mL), kanamycin (50 μg/mL), chloramphenicol (25 μg/mL), and tetracycline (10 μg/mL).

Plasmid and strain construction

Plasmids used in this study were constructed by standard molecular cloning methods. Briefly, PCR products of target genes were inserted into the corresponding vectors by restriction enzyme digestion and ligation or homologous recombination. For heterologous expression, the *sofic* gene was cloned from the genome of *E. coli* E5 and ligated into the pET-28a vector, followed by transformation into DL-TOP10 competent cells for homologous recombination. Point mutations were introduced by inverse PCR, and all constructed plasmids were verified by Sanger sequencing. Verified recombinant plasmids were subsequently transformed into *E. coli* BL21(DE3) for prokaryotic expression.

Gene knockout strains of *E. coli* E5 were constructed using the CRISPR/Cas9 genome editing system. sgRNAs targeting the gene of interest were designed and co-cloned with homologous repair templates into the pSC101-pBAD vector to construct the donor plasmid. The verified donor plasmid and the Cas9 expression plasmid were co-transformed into *E. coli* E5. Successfully transformed recombinants were selected on LB agar plates containing both chloramphenicol and kanamycin. Positive single colonies were inoculated into LB medium containing both antibiotics and cultured at 30°C with shaking until the OD_{600} reached 0.6–0.8. L-arabinose and IPTG were added to induce the expression of sgRNA and Cas9 protein, to achieve targeted cleavage, and the target gene was ultimately deleted via homologous recombination repair. Verification primers were designed upstream and downstream of the

target gene to screen for knockout homozygotes by PCR, and the deletions were confirmed by Sanger sequencing.

Complementation plasmids were generated by standard molecular cloning. A DNA fragment encompassing the native promoter and coding region of sofic was PCR-amplified from *E. coli* E5 genomic DNA and cloned into pBR322 by restriction digestion and ligation or homologous recombination, yielding pBR322-Psofic-sofic, in which sofic expression is driven by its native promoter. Point mutations were introduced by inverse PCR and verified by Sanger sequencing. The sequence-confirmed plasmids were then transformed into competent *E. coli* E5ΔSoFIC cells. Complemented strains were selected with tetracycline (10 μg/mL) and designated *E. coli* E5ΔSoFIC-WT and the mutant-complemented strains *E. coli* E5ΔSoFIC-H264A, *E. coli* E5ΔSoFIC-D268A, *E. coli* E5ΔSoFIC-R272A, and *E. coli* E5ΔSoFIC-H264A/D268A/R272A.

Distribution of SoFIC systems and phylogenetic analysis

Millman et al. predicted defense systems in 3,895 bacterial and archaeal genomes using the DefenseFinder model and identified 629 SoFIC defense systems across 539 bacterial and archaeal genomes[42]. Based on the published gene and genome accession numbers, the genomic information of these 539 species and the 629 SoFIC defense system sequences were downloaded from the JGI IMG database. These sequences were combined with the SoFIC defense system sequences predicted from *E. coli* E5 and *E. coli* H397 by PADLOC and DefenseFinder, resulting in a comprehensive dataset comprising 632 SoFIC defense system protein sequences derived from 541 bacterial and archaeal species (Table S1). The distribution of SoFic proteins at the phylum, order, and genus levels was analyzed based on the information retrieved from the public databases. The length distribution of SoFic proteins was characterized by descriptive statistical analysis, including the calculation of minimum, maximum, and mean values. Multiple sequence alignment of the 632 SoFic protein sequences was performed using the Muscle5 algorithm, and low-quality regions of the alignment were trimmed using ClipKIT. Based on the trimmed alignment matrix, a maximum likelihood phylogenetic tree was constructed using MEGA11 software. The best-fit amino acid substitution model was

automatically selected by the ModelFinder program according to the Bayesian Information Criterion (BIC). The topological reliability of the tree was assessed by 1,000 ultrafast bootstrap replicates. The resulting phylogenetic tree file was uploaded to the iTOL online platform for interactive visualization and graphical refinement.

SoFic protein domain and motif analysis

A systematic structural analysis was performed on SoFic proteins from 13 *E. coli* strains within the dataset(Table S1). Conserved domain annotation of SoFic proteins was carried out using the InterPro platform, integrating prediction results from multiple databases, including Pfam, CDD, and SMART, to determine their domain architecture. Subsequently, three-dimensional structural prediction of the full-length proteins was conducted using AlphaFold3, and the model with the highest prediction confidence was selected as the final structure. Concurrently, the MEME tool was employed to search for highly conserved motifs within the SoFic protein sequences, and these motifs were precisely localized based on multiple sequence alignment results. Molecular visualization and graphical rendering of all three-dimensional protein structural models and the spatial distribution of conserved motifs were performed in PyMOL.

Phage propagation and plaque assays

Bacteriophages used in this study were propagated on their respective host strains and were listed in Table S6. Phages T5, T7, and vB_EcoM_PD205 were amplified on *E. coli* BL21, while phage DE5 was amplified on *E. coli* E5. Phage lysates were filtered through 0.22 μm filters, serially diluted ten-fold, and spotted onto semi-solid agar plates (LB containing 0.75% agar) overlaid with the target bacterial strain. Plates were incubated at 37°C for 5 h (for T5, T7, and vB_EcoM_PD205) or overnight (for DE5), after which plaques were enumerated to calculate plaque-forming units per milliliter (PFU/mL). For the heterologous expression system, the bottom agar was supplemented with 0.1 mM IPTG. *E. coli* BL21(DE3) cells harboring the empty vector or the overexpression plasmid were embedded in the top agar and induced to express the exogenous protein at 37°C for 2 h prior to phage spotting.

Monitoring of phage infection dynamics in liquid culture

E. coli BL21(DE3) overnight cultures carrying the pET-28a-SoFic plasmid or the empty vector were diluted 1:100 (v/v) into fresh LB medium containing kanamycin and incubated at 37°C with shaking at 220 rpm until early logarithmic phase (OD_{600} ≈ 0.3). IPTG was added to a final concentration of 0.5 mM, and the cultures were further incubated at 37°C for 2 h with shaking to induce SoFIC protein expression. Each culture was adjusted to the same OD_{600} value (~0.3) with fresh LB medium, and phage T5 was added at an MOI of 0.01 or 1. Starting immediately after phage addition, 1 mL of culture was aseptically sampled every 20 min for a total duration of 5 h. The optical density at 600 nm (OD_{600}) of each sample was measured using a multifunctional microplate reader.

The procedure for monitoring the infection dynamics of phage DE5 in liquid culture was largely the same as above. Overnight cultures of *E. coli* E5 and *E. coli* E5ΔSoFIC were diluted 1:100 (v/v) into 100 mL of fresh LB medium in 500 mL Erlenmeyer flasks and incubated at 37°C with shaking at 220 rpm until reaching the same OD_{600} value (~0.7). Phage DE5 was added at MOIs of 0.001, 0.01, and 1, respectively. Starting from phage addition, 1 mL of culture was aseptically sampled every 15 min for a total duration of 12 h, and the OD_{600} value was measured using a multifunctional microplate reader. The dynamic curves of OD_{600} values were plotted with culture time as the horizontal axis and OD_{600} as the vertical axis.

Phage propagation titer determination

Overnight cultures of *E. coli* E5 wild-type, single-knockout and double-knockout strains, complemented strains were diluted 1:100 (v/v) into fresh LB medium and incubated at 37°C with shaking until logarithmic phase (OD_{600} ≈ 0.8). The bacterial concentration was adjusted to approximately 1×10^9 CFU/mL. Cultures were aliquoted into sterile tubes, and phage DE5 was added at various multiplicities of infection (MOIs), followed by continuous incubation at 37°C with shaking at 220 rpm. At 1, 3, and 5 hours post-infection, 100 μL of the infected culture was aseptically withdrawn and centrifuged at 12,000 rpm for 2 min at 4°C to collect the supernatant. The supernatant was serially diluted ten-fold and spotted onto semi-solid agar plates (LB containing 0.75% agar) overlaid with *E. coli* E5. Plates were incubated upside down at 37°C overnight (approximately 12–16 h). Phage titers at each time point were calculated

based on the dilution factor and expressed as PFU/mL. The efficiency of plating (EOP) of each knockout strain relative to wild-type *E. coli* E5 was calculated as the ratio of phage titers on the respective strains at the same time point.

Bacterial growth curve measurement

Overnight bacterial cultures were diluted 1:100 (v/v) into 100 mL of fresh LB medium in 500 mL Erlenmeyer flasks and incubated at 37°C with shaking at 220 rpm. Starting from inoculation, 1 mL of culture was aseptically sampled every hour, and the optical density at 600 nm (OD_{600}) was measured using a multifunctional microplate reader. Bacterial growth curves were plotted with culture time as the horizontal axis and OD_{600} as the vertical axis. Experiments were performed independently in triplicate, and results are presented as mean ± standard deviation (SD).

Bacterial lysis rate determination

Overnight bacterial cultures were diluted 1:100 (v/v) into fresh LB medium and incubated at 37°C with shaking to logarithmic phase ($OD_{600} \approx 0.8$). The bacterial concentration was adjusted to approximately 1×10^9 CFU/mL. A 1 mL aliquot of the quantified bacterial culture was infected with phage DE5 at an MOI of 0.01 and incubated at 37°C with shaking at 220 rpm for 3 h. The culture was centrifuged at 12,000 rpm for 2 min to harvest the bacterial pellet, and the supernatant was discarded. The pellet was washed three times with PBS by repeated centrifugation at 12,000 rpm for 2 min, and finally resuspended in 1 mL of fresh LB medium. Bacterial suspensions collected before and after phage infection were serially diluted ten-fold in LB medium, spotted onto LB agar plates, and incubated at 37°C overnight. The bacterial lysis rate was calculated as: [(initial viable count − surviving viable count) / initial viable count] × 100%.

One-step growth curve analysis of phage DE5

Overnight cultures of *E. coli* E5 were diluted 1:100 (v/v) into fresh LB medium and incubated at 37°C with shaking until logarithmic phase ($OD_{600} \approx 0.8$). The bacterial concentration was

adjusted to approximately 1 × 10^8 CFU/mL. A 900 μL aliquot of the bacterial suspension was mixed with 100 μL of phage lysate to achieve a multiplicity of infection (MOI) of 0.01 and incubated at 37°C for 10 min without shaking to allow phage adsorption. After adsorption, the mixture was centrifuged at 12,000 rpm for 5 min at 4°C to remove unadsorbed free phages. The supernatant was discarded, and the pellet was resuspended in 1 mL of PBS, followed by two additional rounds of centrifugation and washing to thoroughly eliminate residual free phages. The final pellet was resuspended in 30 mL of pre-warmed LB medium; this time point was designated as the infection initiation point (t = 0). Starting from t = 0, 200 μL aliquots were aseptically sampled every 10 min, and the phage titer in each sample was immediately quantified by the plaque assay. A one-step growth curve was plotted with infection time as the horizontal axis and the logarithmic value of phage titer (PFU/mL) as the vertical axis. The latent period (the time interval from infection to the first significant increase in extracellular phage titer), the rise phase, and the plateau phase were determined from the curve, and the complete infection cycle was calculated.

Phage adsorption assay

Overnight bacterial cultures were diluted to 1 × 10^8 CFU/mL. A 1 mL aliquot of the bacterial suspension was mixed with phage lysate at an MOI of 0.01. The mixture was incubated statically at 37°C or 4°C, and at designated time points, the mixture was rapidly centrifuged at 12,000 rpm, and the supernatant was collected. The pellet was immediately resuspended in 1 mL of PBS to wash away unadsorbed phages and centrifuged again at 12,000 rpm. The resulting supernatant was combined with the first supernatant. Free unadsorbed phages in the combined supernatant were quantified by the double-layer agar plate method. The adsorption rate was calculated as: [(total initial phage count − free phage count in the supernatant) / total initial phage count] × 100%.

Biofilm formation assay by crystal violet staining

The concentration of overnight *E. coli* cultures was adjusted to 1 × 10^9 CFU/mL and then diluted 1:100 (v/v) into fresh LB medium. A 200 μL aliquot was added to each well of a 96-well cell culture plate (six replicates per bacterial strain) and incubated at 37°C for 48 h under

static conditions. Planktonic bacteria were discarded, and the wells were gently washed three times with PBS to remove non-adherent cells. Subsequently, 200 μL of methanol was added to each well for fixation for 15 min. The methanol fixative was carefully aspirated, and the wells were gently washed once with PBS. Biofilms attached to the well walls were stained with 100 μL of 0.1% (w/v) crystal violet solution for 30 min, followed by washing with PBS to remove excess dye. After air-drying, the bound crystal violet was solubilized with 95% ethanol, and the absorbance was measured at 595 nm using a microplate reader.

Bacterial swimming motility assay

Overnight bacterial cultures were diluted 1:100 (v/v) into fresh LB medium and incubated at 37°C with shaking until OD_{600} reached 0.8. A 1 μL aliquot of the culture was inoculated into the center of LB semi-solid agar plates containing 0.3% (w/v) agar. Plates were incubated upright at 37°C for 24 h under static conditions. The diameter of the bacterial swimming zone was measured to assess motility. Each experiment was performed independently in triplicate.

Transcriptomic analysis (RNA-seq)

Overnight cultures of *E. coli* E5 and *E. coli* E5ΔSoFIC were diluted 1:100 (v/v) into fresh LB medium and incubated at 37°C with shaking at 220 rpm until OD_{600} reached 0.8. Bacterial cells were harvested by centrifugation, and the pellets were snap-frozen in liquid nitrogen. For the phage-infected group, phage DE5 was added at an MOI of 0.01, and incubation was continued at 37°C and 220 rpm for an additional 3 h. Cells were collected by centrifugation at 12,000 rpm for 10 min, washed three times with PBS, and snap-frozen in liquid nitrogen. Total RNA extraction, library construction, rRNA depletion, and Illumina paired-end sequencing were performed by BIOZERON Biotechnology Company. Raw sequencing data were subjected to quality control and filtering using fastp, and the clean reads were aligned to the reference genome using HISAT2. TPM values for each gene were calculated using TPMCalculator. Differential expression analysis was performed using DESeq2 with the screening criteria of $|\log_2(\text{Fold Change})| \geqslant 1$ and FDR $\leqslant 0.05$. GO and KEGG enrichment analyses were performed using the corresponding databases. RNA-seq data were deposited in GEO under accession number GSE333263.

DIA quantitative proteomics

Overnight cultures of *E. coli* E5 and *E. coli* E5ΔSoFIC were diluted 1:100 (v/v) into fresh LB medium and cultured at 37°C with shaking at 220 rpm to OD600 = 0.8. Cells were harvested, resuspended in lysis buffer containing protease and phosphatase inhibitors, sonicated on ice, and centrifuged to collect the supernatant. Protein concentration was determined by BCA assay, and protein integrity was assessed by SDS-PAGE. Equal amounts of protein were digested using the SP3 magnetic bead method. SP3 magnetic beads and 100% acetonitrile were added, followed by incubation at room temperature for 20 min. The beads were washed sequentially with 70% ethanol and 70% acetonitrile, resuspended in 50 mM ammonium bicarbonate, and subjected to reduction with DTT at 55°C for 30 min. Then, CAA, trypsin, and LysC were added, and digestion was performed at 37°C with shaking at 1,500 rpm. Peptides were desalted using a SOLA™ SPE 96-well plate, vacuum-dried, and spiked with iRT standard peptides at a volume ratio of 1:20. LC-MS/MS analysis was performed on a timsTOF HT mass spectrometer using a 15-min liquid chromatography gradient in DIA data acquisition mode. Raw data were searched using DIA-NN software. Trypsin digestion, fixed modification carbamidomethyl (C), and variable modifications oxidation (M) and acetyl (protein N-term) were set, with both PSM and protein FDR set to 0.01, to complete DIA quantitative proteomic analysis. For bioinformatics analysis, proteins identified by DIA-NN were filtered by retaining those with at least one unique peptide, valid values in ≥2 samples across all samples, and a valid value proportion of ≥50% in at least one group. For groups with a valid value proportion ≥50%, missing values were filled with the group mean; the remaining missing values were filled with half of the global minimum. Subsequently, median normalization and log2 transformation were performed. Quality control was conducted using principal component analysis (PCA), sample correlation analysis, and hierarchical clustering. Differentially expressed proteins were screened using a threshold of FC ≥ 2 or FC ≤ 1/2. t-tests were used for two-group comparisons, and ANOVA was used for multi-group comparisons.

SoFic protein purification and pull-down assay

The SoFic protein-coding gene fused with an N-terminal His-tag was cloned into the pET-28a-empty vector and transformed into *E. coli* TOP10 competent cells. Positive monoclonal colonies were identified by kanamycin resistance screening and PCR verification, and further confirmed by Sanger sequencing. The verified recombinant plasmid was extracted and transformed into *E. coli* BL21(DE3) for prokaryotic expression. The bacterial culture was diluted 1:100 (v/v) into kanamycin-containing LB medium and incubated at 37°C with shaking at 220 rpm until logarithmic phase. Protein expression was induced by adding 0.01 mM IPTG and incubating at 16°C with shaking at 160 rpm overnight. Bacterial cells were disrupted by ultrasonication, and the inclusion body precipitate was collected. The inclusion bodies were dissolved and refolded using a urea gradient (8 M, 6 M, 4 M, 2 M, and 1 M urea). The refolded His-SoFic protein mixture was equally divided and loaded onto two Ni-NTA agarose resin columns (Qiagen) for affinity chromatography purification. Following sample loading and washing with a low-concentration imidazole (20 mM) buffer to remove non-specifically bound proteins while retaining His-SoFic on the column, the resin was incubated with *E. coli* E5 whole-cell lysate or *E. coli* E5 whole-cell lysate stimulated with phage DE5 for 1 h at 4°C with gentle rotation for 2 h. After washing with low-concentration imidazole (20 mM) buffer to remove non-specifically bound proteins, the His-SoFic protein and its binding partners were eluted from the Ni-NTA agarose resin with a high-concentration imidazole (250 mM) buffer. The eluate was separated by SDS-PAGE, and the entire lane was excised for liquid chromatography-tandem mass spectrometry (LC-MS/MS) identification. Specific interacting proteins of the SoFIC defense system upon DE5 phage stimulation were identified by comparative analysis.

Transmission electron microscopy (TEM) observation

For negative staining, samples of *E. coli* E5, *E. coli* E5ΔSoFIC, *E. coli* E5ΔSoFIC-WT and *E. coli* E5ΔSoFIC-H264A/D268A/R272A strains were prepared by applying 10 μL of the bacterial suspension onto a copper grid and allowing it to settle for 1 min. Excess liquid was removed with filter paper. Subsequently, 10 μL of phosphotungstic acid staining solution was applied to the grid and allowed to settle for 1 min, after which excess liquid was removed with filter paper. The grids were air-dried at room temperature for several minutes. Bacterial morphology was

observed using a Hitachi HT7800 transmission electron microscope operated at an accelerating voltage of 120 kV, and images were acquired for analysis.

For *E. coli* E5 and *E. coli* E5ΔSoFIC strains infected with phage DE5 at an MOI of 0.01 for 50 min and 3 h, samples were prepared by the resin-embedding ultrathin sectioning method. At 50 min and 3 h post-infection, bacterial cultures were collected by centrifugation at 12,000 rpm for 5 min at 4°C, and the supernatant was discarded. The pellets were immediately fixed with 2.5% glutaraldehyde at 4°C for 16 h. The fixed samples were rinsed three times with 0.1 M phosphate buffer (PB, pH 7.35), 15 min each. Post-fixation was performed with 1% osmium tetroxide solution for 1–2 h. The osmium tetroxide waste solution was carefully removed, and the samples were rinsed with 0.1 M phosphate buffer (PB, pH 7.35) for 15 min, followed by three washes with distilled water, 10 min each. The samples were dehydrated through a graded ethanol series (30%, 50%, 70%, 80%, 95%, and 100% ethanol) for 15 min each, followed by three changes of 100% propylene oxide, 15 min each. The dehydrated samples were infiltrated and embedded in epoxy resin. The infiltration steps were as follows: propylene oxide: embedding medium = 1:1 at room temperature for 2 h; propylene oxide: embedding medium = 1:2 overnight; pure embedding medium at room temperature for 4 h, repeated twice. The pure embedding medium was poured into embedding molds, and the samples were inserted into the molds, followed by polymerization at 37°C for 48 h and 45°C for 12 h. The embedding molds were then placed in a 60°C oven for 48 h for final polymerization, and the resulting resin blocks were retrieved. Ultrathin sections (60–70 nm) were cut from the resin blocks using an ultramicrotome and collected onto copper grids. The sections were stained with uranyl acetate for 10–30 min, washed with water, stained with lead citrate for 7 min, washed with water, air-dried, and observed. The ultrastructure of the samples was observed using a transmission electron microscope (JEOL 1400Flash) operated at an accelerating voltage of 80 kV, and digital images were acquired using the accompanying CCD camera. Observations focused on the integrity of the bacterial cell wall and cell membrane, changes in the cytoplasmic matrix, and the assembly status and distribution of intracellular phage particles.

Statistical analysis

Unless otherwise specified, all experiments were performed independently in triplicate, and results are presented as mean ± standard deviation (SD). All statistical analyses and graphical representations were performed using GraphPad Prism 10.1.2 software.

Supplementary Materials: All supplementary files are available in the submission system.

Author Contributions: Conceptualization, Q J and JH H; methodology, Q J, and BX Y; software, Q J; validation, Q J, BX Y, and JH H; data analysis, Q J, and JH H; investigation, Q J, BX Y, SY G, SC Z, Y L, LL Z and DP H; resources, JH H; data curation, Q J, XB F; writing—original draft preparation, Q J, and JH H; writing—review and editing, Q J, and JH H; visualization, Q J; supervision, JH H; project administration, JH H; funding acquisition, JH H. All authors have read and agreed to the published version of the manuscript.

Funding: The work was supported by the Tianjin Key Science and Technology Support Project (24YFZCSN00180), Jingjinji Collaborative Research Program (25JJJC0018) and Tianjin Municipal Major Science and Technology Projects and Engineering（25ZXCKQY00020）.

Informed Consent Statement: Not applicable.

Data Availability Statement: The data supporting the findings of this study are available from the corresponding author upon reasonable request. The genome sequence and transcriptomic data will be deposited in public databases upon acceptance of the manuscript.

Conflicts of Interest: The authors declare no conflicts of interest.

References

[1] KOSKELLA B, HERNANDEZ C A, WHEATLEY R M. Understanding the Impacts of Bacteriophage Viruses: From Laboratory Evolution to Natural Ecosystems [J]. Annu Rev Virol, 2022, 9(1): 57-78.

[2] GEORJON H, BERNHEIM A. The highly diverse antiphage defence systems of bacteria [J]. Nat Rev Microbiol, 2023, 21(10): 686-700.

[3] WU Y, GARUSHYANTS S K, VAN DEN HURK A, et al. Bacterial defense systems exhibit synergistic anti-phage activity [J]. Cell Host Microbe, 2024, 32(4): 557-72.e6.

[4] MURTAZALIEVA K, MU A, PETROVSKAYA A, et al. The growing repertoire of phage anti-defence systems [J]. Trends Microbiol, 2024, 32(12): 1212-28.

[5] AGAPOV A, BAKER K S, BEDEKAR P, et al. Multi-layered genome defences in bacteria [J]. Curr Opin Microbiol, 2024, 78(102436.

[6] AMYX-SHERER K, AWASTHI L C, ZHENG A, et al. Two unrelated Pseudomonas aeruginosa phages require the exopolysaccharide Psl for infection [J]. NPJ Biofilms Microbiomes, 2025, 11(1): 211.

[7] VIDAKOVIC L, SINGH P K, HARTMANN R, et al. Dynamic biofilm architecture confers individual and collective mechanisms of viral protection [J]. Nat Microbiol, 2018, 3(1): 26-31.

[8] ROBERTS C G, FISHMAN C B, ZHANG Z, et al. Bacterial TIR-based immune systems sense phage capsids to initiate defense [J]. Nat Microbiol, 2025, 10(11): 2892-902.
[9] WANG J, LI Z, LANG H, et al. Cyclic-dinucleotide-induced filamentous assembly of phospholipases governs broad CBASS immunity [J]. Cell, 2025, 188(14): 3744-56.e16.
[10] KANG H, GAO A, ZHU Y. Bacterial restriction-modification systems: mechanisms of defense against phage infection [J]. Biophys Rep, 2025, 11(5): 330-43.
[11] IBRAHIM R, ARANJANI J M. Bacterial defense mechanisms against bacteriophages: an evolutionary arms race [J]. Arch Microbiol, 2026, 208(5):
[12] WATSON B N J, STEENS J A, STAALS R H J, et al. Coevolution between bacterial CRISPR-Cas systems and their bacteriophages [J]. Cell Host Microbe, 2021, 29(5): 715-25.
[13] SKLIROS D, DROUBOGIANNIS S, KALLONIATI C, et al. Perturbation of Quorum Sensing after the Acquisition of Bacteriophage Resistance Could Contribute to Novel Traits in Vibrio alginolyticus [J]. Microorganisms, 2023, 11(9):
[14] OU J, ZHANG S, ZHANG M, et al. Responding to exogenous quorum-sensing signals promotes defense against phages by repressing OmpV expression in Pseudomonas syringae pv. actinidiae [J]. Microbiol Res, 2025, 293(128074.
[15] WANG X, LEPTIHN S. Defense and anti-defense mechanisms of bacteria and bacteriophages [J]. J Zhejiang Univ Sci B, 2024, 25(3): 181-96.
[16] BEAVOGUI A, LACROIX A, WIART N, et al. The defensome of complex bacterial communities [J]. Nat Commun, 2024, 15(1): 2146.
[17] BONDY-DENOMY J, QIAN J, WESTRA E R, et al. Prophages mediate defense against phage infection through diverse mechanisms [J]. Isme j, 2016, 10(12): 2854-66.
[18] PEDRUZZI I, ROSENBUSCH J P, LOCHER K P. Inactivation in vitro of the Escherichia coli outer membrane protein FhuA by a phage T5-encoded lipoprotein [J]. FEMS Microbiol Lett, 1998, 168(1): 119-25.
[19] HARVEY H, BONDY-DENOMY J, MARQUIS H, et al. Pseudomonas aeruginosa defends against phages through type IV pilus glycosylation [J]. Nat Microbiol, 2018, 3(1): 47-52.
[20] CHUNG I Y, JANG H J, BAE H W, et al. A phage protein that inhibits the bacterial ATPase required for type IV pilus assembly [J]. Proc Natl Acad Sci U S A, 2014, 111(31): 11503-8.
[21] SCHOLL D, ADHYA S, MERRIL C. Escherichia coli K1's capsule is a barrier to bacteriophage T7 [J]. Appl Environ Microbiol, 2005, 71(8): 4872-4.
[22] GORDILLO ALTAMIRANO F, FORSYTH J H, PATWA R, et al. Bacteriophage-resistant Acinetobacter baumannii are resensitized to antimicrobials [J]. Nat Microbiol, 2021, 6(2): 157-61.
[23] ZHANG Z, TODESCHINI T C, WU Y, et al. Kiwa is a membrane-embedded defense supercomplex activated at phage attachment sites [J]. Cell, 2025, 188(21): 5862-77.e23.
[24] LABRIE S J, SAMSON J E, MOINEAU S. Bacteriophage resistance mechanisms [J]. Nat Rev Microbiol, 2010, 8(5): 317-27.
[25] NASRULLAH, HUSSAIN A, AHMED S, et al. DNA methylation across the tree of life, from micro to macro-organism [J]. Bioengineered, 2022, 13(1): 1666-85.
[26] VAN HOUTE S, BUCKLING A, WESTRA E R. Evolutionary Ecology of Prokaryotic Immune Mechanisms [J]. Microbiol Mol Biol Rev, 2016, 80(3): 745-63.
[27] MO C Y, MATHAI J, ROSTøL J T, et al. Type III-A CRISPR immunity promotes mutagenesis of staphylococci [J]. Nature, 2021, 592(7855): 611-5.
[28] LI Y, BONDY-DENOMY J. Anti-CRISPRs go viral: The infection biology of CRISPR-Cas

inhibitors [J]. Cell Host Microbe, 2021, 29(5): 704-14.
[29] BONDY-DENOMY J, PAWLUK A, MAXWELL K L, et al. Bacteriophage genes that inactivate the CRISPR/Cas bacterial immune system [J]. Nature, 2013, 493(7432): 429-32.
[30] LOEFF L, WALTER A, ROSALEN G T, et al. DNA end sensing and cleavage by the Shedu anti-phage defense system [J]. Cell, 2025, 188(3): 721-33.e17.
[31] BRAVO J P K, APARICIO-MALDONADO C, NOBREGA F L, et al. Structural basis for broad anti-phage immunity by DISARM [J]. Nat Commun, 2022, 13(1): 2987.
[32] JOHNSON A G, WEIN T, MAYER M L, et al. Bacterial gasdermins reveal an ancient mechanism of cell death [J]. Science, 2022, 375(6577): 221-5.
[33] HAUDIQUET M, CHAKRAVARTI A, ZHANG Z, et al. Structural basis for Lamassu-based antiviral immunity and its evolution from DNA repair machinery [J]. bioRxiv, 2025,
[34] WANG L, ZHANG L. The arms race between bacteria CBASS and bacteriophages [J]. Front Immunol, 2023, 14(1224341.
[35] TAMULAITIENE G, SABONIS D, SASNAUSKAS G, et al. Activation of Thoeris antiviral system via SIR2 effector filament assembly [J]. Nature, 2024, 627(8003): 431-6.
[36] ZENG Z, HU Z, ZHAO R, et al. Base-modified nucleotides mediate immune signaling in bacteria [J]. Science, 2025, 388(6745): eads6055.
[37] ROY C R, CHERFILS J. Structure and function of Fic proteins [J]. Nat Rev Microbiol, 2015, 13(10): 631-40.
[38] HARMS A, STANGER F V, DEHIO C. Biological Diversity and Molecular Plasticity of FIC Domain Proteins [J]. Annu Rev Microbiol, 2016, 70(341-60.
[39] LUONG P, KINCH L N, BRAUTIGAM C A, et al. Kinetic and structural insights into the mechanism of AMPylation by VopS Fic domain [J]. J Biol Chem, 2010, 285(26): 20155-63.
[40] SONG P, CHEN T, WANG M, et al. Crystal structure of the Klebsiella pneumoniae fic toxin-antitoxin complex reveals a noncanonical FicT lacking AMPylation activity [J]. Biochem Biophys Res Commun, 2025, 771(152002.
[41] MARIANO G, BLOWER T R. Conserved domains can be found across distinct phage defence systems [J]. Mol Microbiol, 2023, 120(1): 45-53.
[42] MILLMAN A, MELAMED S, LEAVITT A, et al. An expanded arsenal of immune systems that protect bacteria from phages [J]. Cell Host Microbe, 2022, 30(11): 1556-69.e5.
[43] ZHAO J, ZHU Y, WANG C, et al. Simultaneous inhibition of bacterial virulence and anti-phage defense systems by synergistic bacteriophage counter-defense proteins [J]. Embo j, 2026, 45(8): 2756-84.
[44] https://defensefinder.mdmlab.fr/wiki/defense-systems/sofic
[45] https://padloc.otago.ac.nz/padloc/
[46] JASKóLSKA M, ADAMS D W, BLOKESCH M. Two defence systems eliminate plasmids from seventh pandemic Vibrio cholerae [J]. Nature, 2022, 604(7905): 323-9.
[47] WANG H, JOFFRé E. Plasmid copy number as a modulator in bacterial pathogenesis and antibiotic resistance [J]. NPJ Antimicrob Resist, 2025, 3(1): 72.
[48] AFRAMIAN N, OMER BENDORI S, HEN T, et al. Expression level of anti-phage defence systems controls a trade-off between protection range and autoimmunity [J]. Nat Microbiol, 2025, 10(8): 1954-62.
[49] STERN A, KEREN L, WURTZEL O, et al. Self-targeting by CRISPR: gene regulation or autoimmunity? [J]. Trends Genet, 2010, 26(8): 335-40.

[50] PALANIVELU D V, GOEPFERT A, MEURY M, et al. Fic domain-catalyzed adenylylation: insight provided by the structural analysis of the type IV secretion system effector BepA [J]. Protein Sci, 2011, 20(3): 492-9.
[51] CAMPANACCI V, MUKHERJEE S, ROY C R, et al. Structure of the Legionella effector AnkX reveals the mechanism of phosphocholine transfer by the FIC domain [J]. Embo j, 2013, 32(10): 1469-77.
[52] GOEPFERT A, STANGER F V, DEHIO C, et al. Conserved inhibitory mechanism and competent ATP binding mode for adenylyltransferases with Fic fold [J]. PLoS One, 2013, 8(5): e64901.
[53] XIAO J, WORBY C A, MATTOO S, et al. Structural basis of Fic-mediated adenylylation [J]. Nat Struct Mol Biol, 2010, 17(8): 1004-10.
[54] KLEMM P. Two regulatory fim genes, fimB and fimE, control the phase variation of type 1 fimbriae in Escherichia coli [J]. Embo j, 1986, 5(6): 1389-93.
[55] ROBINSON L S, ASHMAN E M, HULTGREN S J, et al. Secretion of curli fibre subunits is mediated by the outer membrane-localized CsgG protein [J]. Mol Microbiol, 2006, 59(3): 870-81.
[56] CUI J, ZHONG W, LIU W, et al. Whole genome sequencing and annotation of a lysogenic phage vB_EcoP_DE5 isolated from donkey-derived Escherichia coli [J]. Virus Genes, 2023, 59(2): 290-300.
[57] ŠIBOROVá M, FüZIK T, PROCHáZKOVá M, et al. Tail proteins of phage SU10 reorganize into the nozzle for genome delivery [J]. Nat Commun, 2022, 13(1): 5622.
[58] https://cge.food.dtu.dk/services/SerotypeFinder/)
[59] YANG B, SENCHENKOVA S N, NAUMENKO O I, et al. Structural and genetic relatedness of the O-antigens of Escherichia coli O50 and O2 [J]. Carbohydr Res, 2018, 464(8-11.
[60] SHINDO H, FURUBAYASHI A, SHIMIZU M, et al. Preferential binding of E.coli histone-like protein HU alpha to negatively supercoiled DNA [J]. Nucleic Acids Res, 1992, 20(7): 1553-8.
[61] LI S, WATERS R. Escherichia coli strains lacking protein HU are UV sensitive due to a role for HU in homologous recombination [J]. J Bacteriol, 1998, 180(15): 3750-6.
[62] BAQUERO M R, BOUZON M, VAREA J, et al. sbmC, a stationary-phase induced SOS Escherichia coli gene, whose product protects cells from the DNA replication inhibitor microcin B17 [J]. Mol Microbiol, 1995, 18(2): 301-11.
[63] SWINDLE J, ZYLICZ M, GEORGOPOULOS C, et al. Purification and properties of the NusB protein of Escherichia coli [J]. J Biol Chem, 1988, 263(21): 10229-35.
[64] NAVRE M, SCHACHMAN H K. Synthesis of aspartate transcarbamoylase in Escherichia coli: transcriptional regulation of the pyrB-pyrI operon [J]. Proc Natl Acad Sci U S A, 1983, 80(5): 1207-11.
[65] ANDREWS S C, ROBINSON A K, RODRíGUEZ-QUIñONES F. Bacterial iron homeostasis [J]. FEMS Microbiol Rev, 2003, 27(2-3): 215-37.
[66] WEISSBACH H, ETIENNE F, HOSHI T, et al. Peptide methionine sulfoxide reductase: structure, mechanism of action, and biological function [J]. Arch Biochem Biophys, 2002, 397(2): 172-8.
[67] ALIAGA-TOBAR V, TORRES J, MENDOZA S N, et al. Reduced glutathione levels in Enterococcus faecalis trigger metabolic and transcriptional compensatory adjustments during iron exposure [J]. mSystems, 2026, 11(1): e0124025.
[68] DORON S, MELAMED S, OFIR G, et al. Systematic discovery of antiphage defense systems

in the microbial pangenome [J]. Science, 2018, 359(6379):
[69] KLEIN-SOUSA V, ROA-EGUIARA A, KIELKOPF C S, et al. RBPseg: Toward a complete phage tail fiber structure atlas [J]. Sci Adv, 2025, 11(23): eadv0870.
[70] NOBREGA F L, VLOT M, DE JONGE P A, et al. Targeting mechanisms of tailed bacteriophages [J]. Nat Rev Microbiol, 2018, 16(12): 760-73.
[71] DAVISON J. Pre-early functions of bacteriophage T5 and its relatives [J]. Bacteriophage, 2015, 5(4): e1086500.
[72] KULCZYK A W, RICHARDSON C C. The Replication System of Bacteriophage T7 [J]. Enzymes, 2016, 39(89-136.

Figure legends

Figure 1. SoFIC defense systems are widely distributed across bacteria and exhibit diverse sequence features.

(A) Prevalence of the SoFIC defense system across 22,818 complete prokaryotic genomes. The percentage of genomes containing at least one SoFIC system is indicated (9.91%).

(B) Phylogenetic tree reconstructed from 632 SoFic protein sequences derived from 541 bacterial and archaeal species.

(C) Distribution of SoFIC systems across major bacterial phyla. Proteobacteria account for the largest proportion (68.39%), followed by Fusobacteria, Cyanobacteria, Spirochaetes, and Bacteroidetes.

(D) Further subdivision of SoFIC systems within Proteobacteria. From left to right, the distribution is shown across orders within Proteobacteria, families within Enterobacterales, and genera within the family Enterobacteriaceae.

(E) Size distribution of SoFic proteins. The lengths range from 195 to 455 amino acids.

(F) Copy number distribution of SoFIC defense systems per bacterial genome.

Figure 2. Architecture of SoFIC anti-phage defense systems

(A) Domain architectures of representative SoFic proteins from 13 *E. coli* strains. Three types were identified: SoFic proteins represented by *E. coli* SF-166 contain a Fic_N domain, a Fic domain, and a SoFic-like_C domain; SoFic proteins represented by *E. coli* S10 contain Fic_N and Fic domains but lack the SoFic-like_C domain; SoFic proteins represented by *E. coli* E5 contain only the core Fic domain.

(B) Three-dimensional structural models of the three representative SoFic proteins predicted by AlphaFold3, showing distinct domain organizations.

(C) Protein motif prediction of the three representative SoFic proteins. A continuous highly conserved region of 37 amino acids was identified within the Fic domain, and the canonical FIC motif (HPF(P/R)DGNGR) was recognized at positions 16 to 24 of this conserved region.

(D) Schematic representation of the conserved FIC motif showing key catalytic residues. The conserved histidine (H), arginine (R), and aspartate (D) residues were

highlighted in red, while other conserved residues were highlighted in blue, green, yellow.

Figure 3. SoFIC confers anti-phage immunity in the heterologous expression system.

(A) Schematic representation of the heterologous expression system. The sofic gene from *E. coli* E5 was cloned into the pET-28a vector and overexpressed in *E. coli* BL21(DE3), which naturally lacks the SoFIC defense system.

(B–E) Anti-phage activity of SoFIC against three representative phages. SoFIC conferred strong resistance against the long-tail phage T5, weak resistance against the short-tail phage T7, and no detectable resistance against the myophage vB_EcoM_PD205. Empty vector controls are shown for comparison. Single mutations (H264A, D268A, R272A) and the triple mutation (H264A/D268A/R272A) of the key catalytic residues almost completely abolished the anti-phage activity of SoFIC.

(F) Dynamic changes in OD_{600} of bacterial cultures after T5 infection at different multiplicities of infection (MOIs). SoFIC effectively protected the host at a low MOI (0.01) but was overwhelmed at a high MOI (1).

Figure 4. SoFIC-mediated anti-phage defense in the native host requires an intact Fic motif.

(A) One-step growth curve of phage DE5, showing a complete infection cycle of approximately 1 h.

(B) Spot assays showing phage titers at 1, 3, and 5 h post-infection with DE5 at MOIs of 0.001, 0.01, 1, and 10 in *E. coli* E5, E5ΔSoFIC, and complemented strains (E5ΔSoFIC-WT, E5ΔSoFIC-H264A, E5ΔSoFIC-D268A, E5ΔSoFIC-R272A, E5ΔSoFIC-H264A/D268A/R272A).

(C) Dynamic changes in OD_{600} of bacterial cultures after DE5 infection. The ΔSoFIC culture lysed more rapidly, confirming increased susceptibility.

(D) Spot assays of initial CFU and CFU at 3 h post-infection for the indicated strains.
(E) Bacterial lysis rate at 3 h post-infection. Data are presented as mean ± SD.

Figure 5. SoFIC maintains surface architecture and limits phage adsorption in a Fic motif-dependent manner.

(A) Growth curves of *E. coli* E5, E5ΔSoFIC, and complemented strains over 24 h.

(B) Negative-staining transmission electron microscopy images of WT, ΔSoFIC, ΔSoFIC-WT, and ΔSoFIC-3Mut (H264A/D268A/R272A) cells.

(C) Transcriptional analysis of fimbrial gene clusters (fim, csg, pap, sfa, ecp). Most genes were significantly downregulated in the ΔSoFIC strain.

(D) Heatmap of protein abundance (log2(FC)) of fimbria-related proteins in *E. coli* E5 and E5ΔSoFIC.

(E) MA plot of differentially expressed proteins from DIA proteomics. FimB, CsgG, and CsgD are indicated.

(F) Adsorption efficiency of phage DE5 on the indicated strains at 37°C (left) and 4°C (right).

(G) Host range analysis of phage DE5 on the indicated bacterial strains. DE5 efficiently infected *E. coli* E5 and *E. coli* E5ΔSoFIC, but failed to infect *E. coli* E5ΔWaaL or *E. coli* BL21.

(H) Schematic representation of DE5 phage binding to the O2/O50 receptor on the outer membrane of *E. coli* E5. The O-antigen serves as the essential receptor for phage adsorption.

Figure 6. SoFIC remodels host metabolism and prevents phage-induced metabolic collapse through multi-target protein interactions.

(A) Overall gene expression levels in wild-type and ΔSoFIC strains at 3 h post-infection with DE5 (MOI = 0.01).

(B) Number of differentially expressed genes ($|\log FC| \geq 1$, FDR ≤ 0.05). The ΔSoFIC strain showed 163 upregulated and 162 downregulated genes compared to wild-type.

(C) Mass spectrometry analysis of pull-down assays identifying host proteins that specifically interact with SoFic upon DE5 stimulation. Twelve specific interactors were identified.

(D) List of the 12 specific interactors.

(E) Transmission electron microscopy images of wild-type and ΔSoFIC strains at 50 min and 3 h post-infection (MOI = 0.01). At 50 min, ΔSoFIC strains already

showed extensive cell lysis and abundant fully assembled phage particles, whereas wild-type cells remained largely intact. At 3 h, ΔSoFIC strains exhibited massive lysis and numerous phages around cell debris, indicating conversion of the intracellular environment into a "phage factory." High-magnification images (60,000×) reveal structurally intact phages inside ΔSoFIC strains.

Figure 7. SoFIC exhibits intricate functional crosstalk with other bacterial defense systems in a time-dependent manner.

(A) Growth curves of wild-type *E. coli* E5 and various single- and double-knockout strains. Knocking out the Lmuc component of Lamassu_Fam severely impaired bacterial growth, and knockout of the RM I system was synthetically lethal. Simultaneous deletion of SoFIC and other defense systems (except RM I and Lamassu_Fam) did not severely affect growth.

(B) Schematic of the experimental design for measuring efficiency of plating (EOP) after infection with DE5 phage (MOI = 0.01) at 1, 3, and 5 h.

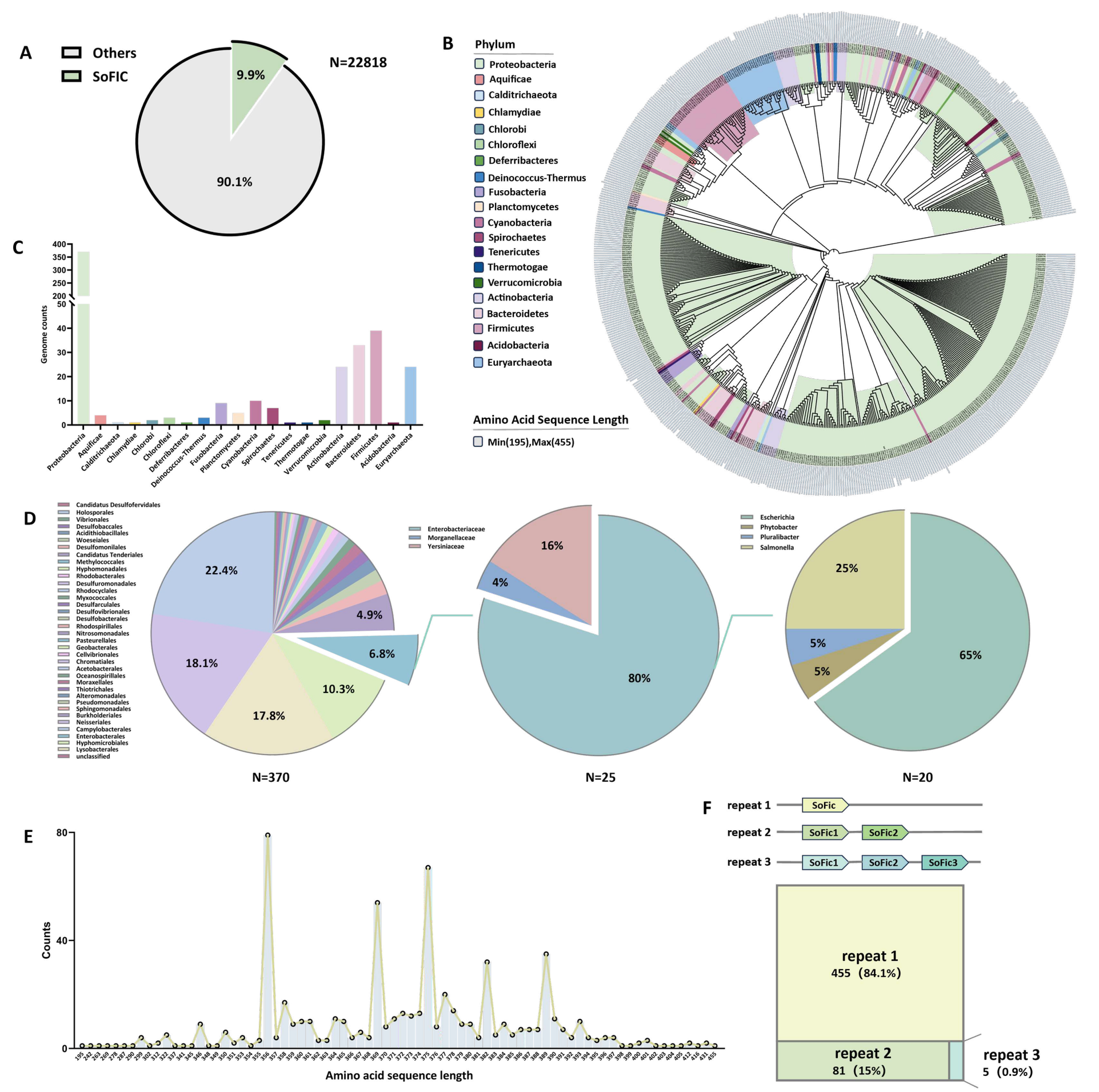
(C) EOP values (fold change relative to wild-type) for single- and double-knockout strains at 1, 3, and 5 h.

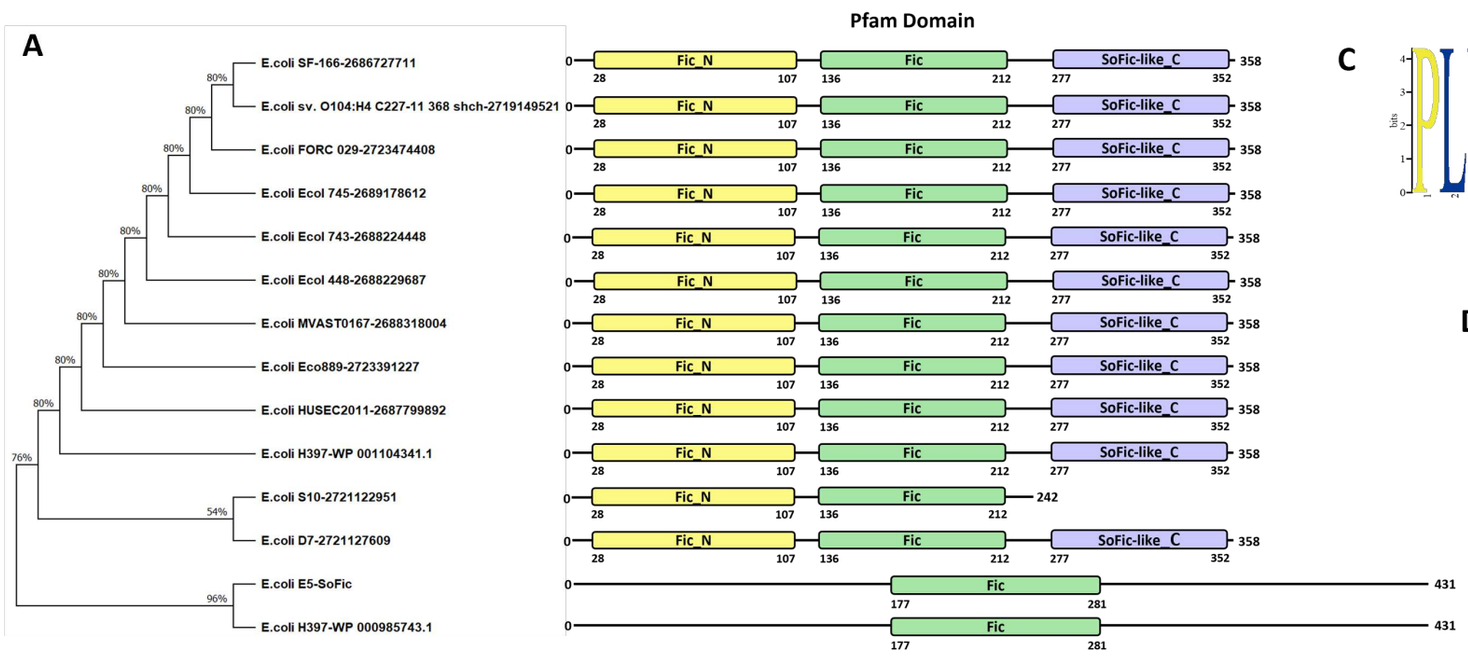
(D) Colony-forming unit (CFU) counts for wild-type and all single- and double-knockout strains before and at 3 h after DE5 phage infection (MOI = 0.01).

(E) Bacterial lysis rates at 3 h post-infection.

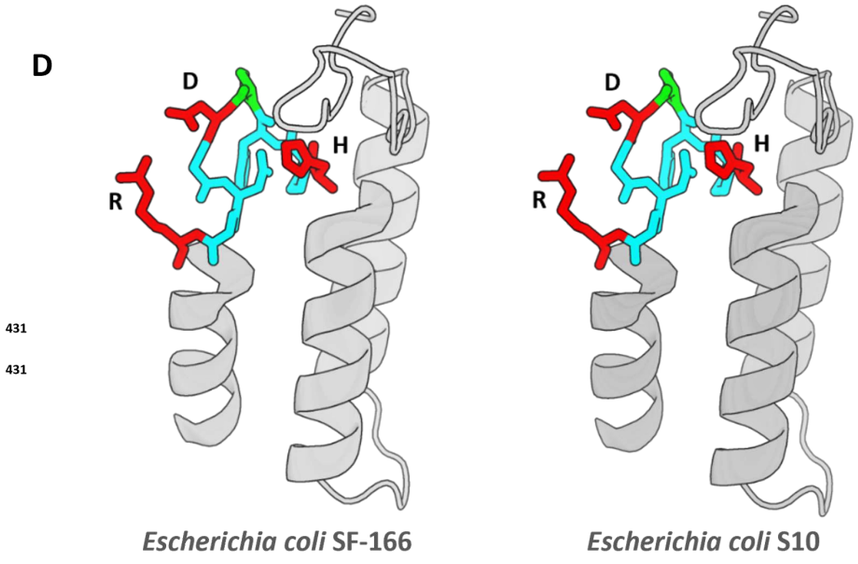
Figure 8. The dual-layer model of the SoFIC defense system in *Escherichia coli* E5 to resist phages.

Extracellularly, SoFIC physically hinders initial phage adsorption by maintaining surface structures such as fimbriae and biofilms. Intracellularly, upon phage genome injection, SoFIC specifically interacts with key host proteins involved in DNA homeostasis (HupA, SbmC), transcription elongation (NusB), nucleotide metabolism (PyrB), and oxidative stress defense (Bfr, MsrA), preventing the host cell from entering a metabolic state conductive to phage proliferation.


A
Others
SoFIC
9.9%
90.1%
N=22818
B
Phylum
Proteobacteria
Aquificae
Calditrichaeota
Chlamydiae
Chlorobi
Chloroflexi
Deferribacteres
Deinococcus-Thermus
Fusobacteria
Planctomycetes
Cyanobacteria
Spirochaetes
Tenericutes
Thermotogae
Verrucomicrobia
Actinobacteria
Bacteroidetes
Firmicutes
Acidobacteria
Euryarchaeota
Amino Acid Sequence Length
Min(195),Max(455)
C
Genome counts
D
Candidatus Desulfofervidales
Holosporales
Vibrionales
Desulfobaccales
Acidithiobacillales
Woeseiales
Desulfomonilales
Candidatus Tenderiales
Methylococcales
Hyphomonadales
Rhodobacterales
Desulfuromonadales
Rhodocyclales
Myxococcales
Desulfarculales
Desulfovibrionales
Desulfobacterales
Rhodospirillales
Nitrosomonadales
Pasteurellales
Geobacterales
Cellvibrionales
Chromatiales
Acetobacterales
Oceanospirillales
Moraxellales
Thiotrichales
Alteromonadales
Pseudomonadales
Sphingomonadales
Burkholderiales
Neisseriales
Campylobacterales
Enterobacterales
Hyphomicrobiales
Lysobacterales
unclassified
22.4%
4.9%
6.8%
10.3%
17.8%
18.1%
N=370
Enterobacteriaceae
Morganellaceae
Yersiniaceae
16%
4%
80%
N=25
Escherichia
Phytobacter
Pluralibacter
Salmonella
25%
5%
5%
65%
N=20
E
Counts
Amino acid sequence length
F
repeat 1
SoFic
repeat 2
SoFic1
SoFic2
repeat 3
SoFic1
SoFic2
SoFic3
repeat 1
455 (84.1%)
repeat 2
81 (15%)
repeat 3
5 (0.9%)

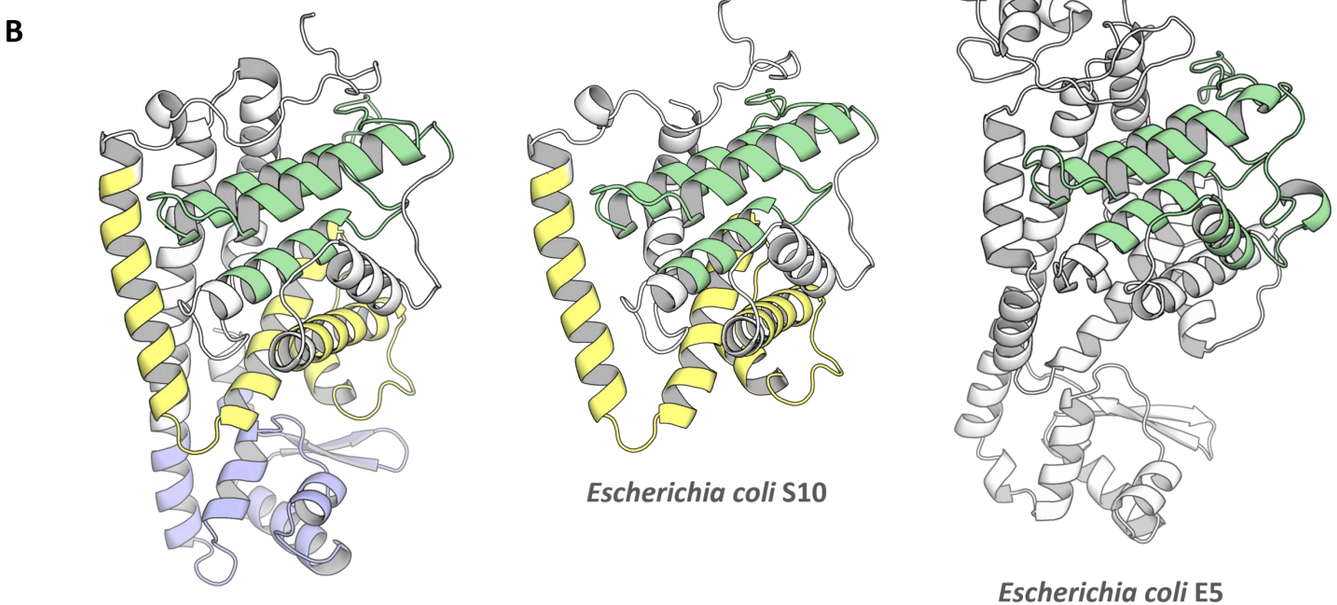






Escherichia coli SF-166

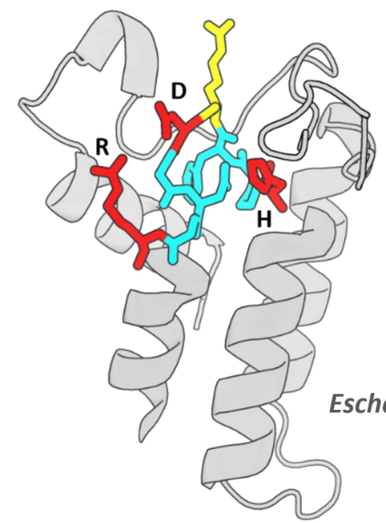
Escherichia coli S10



Escherichia coli SF-166

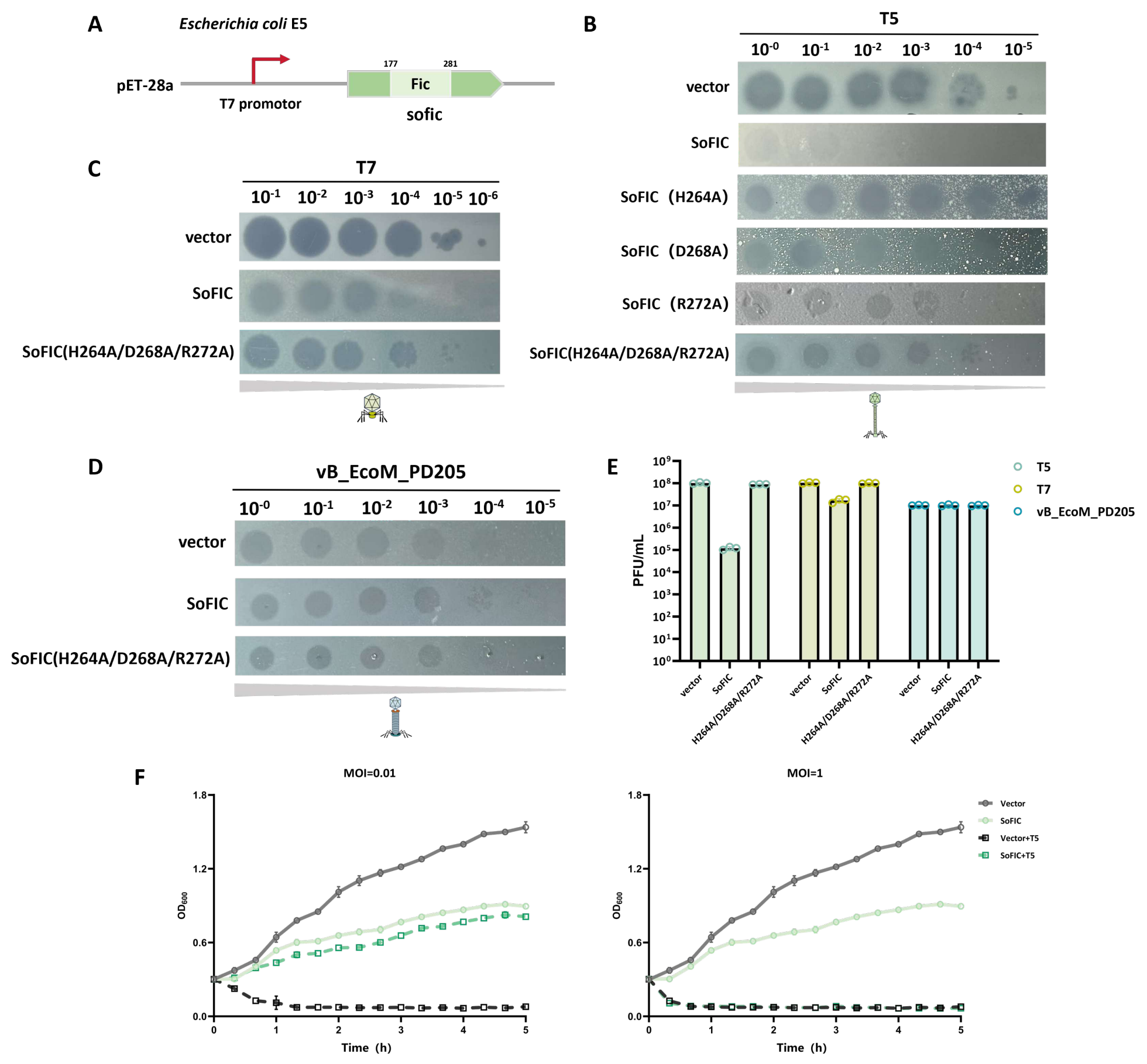
Escherichia coli S10

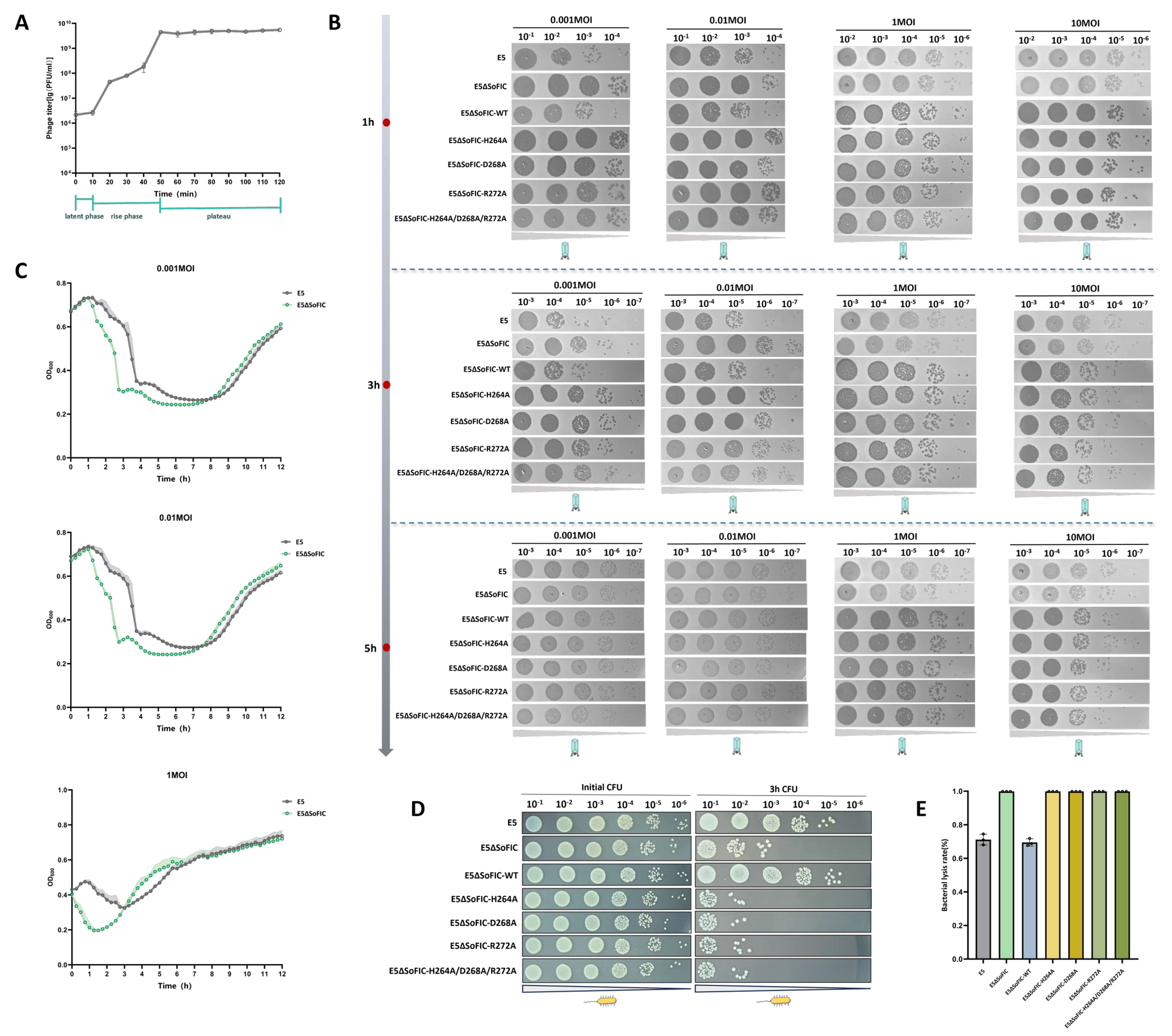
Escherichia coli E5

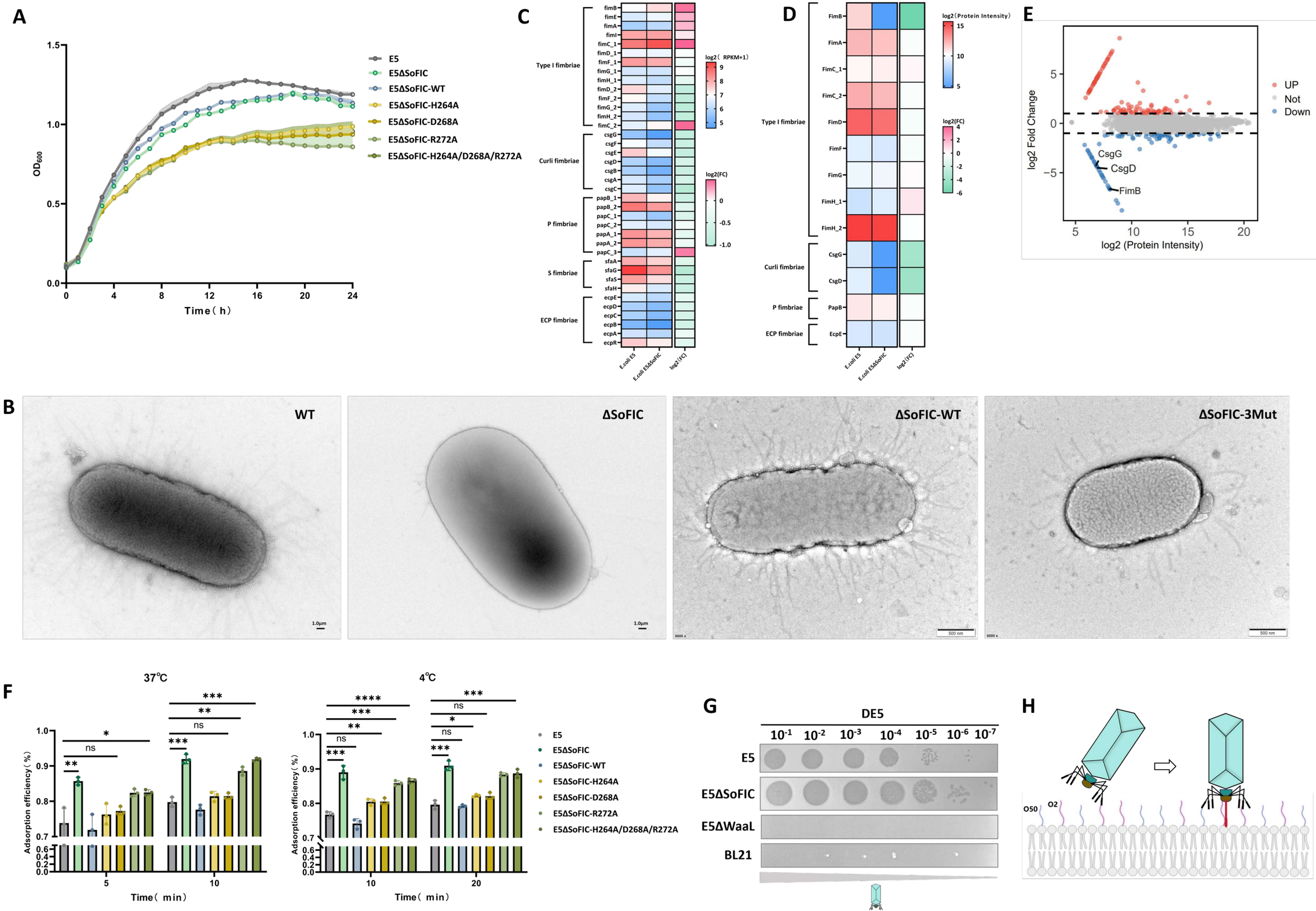


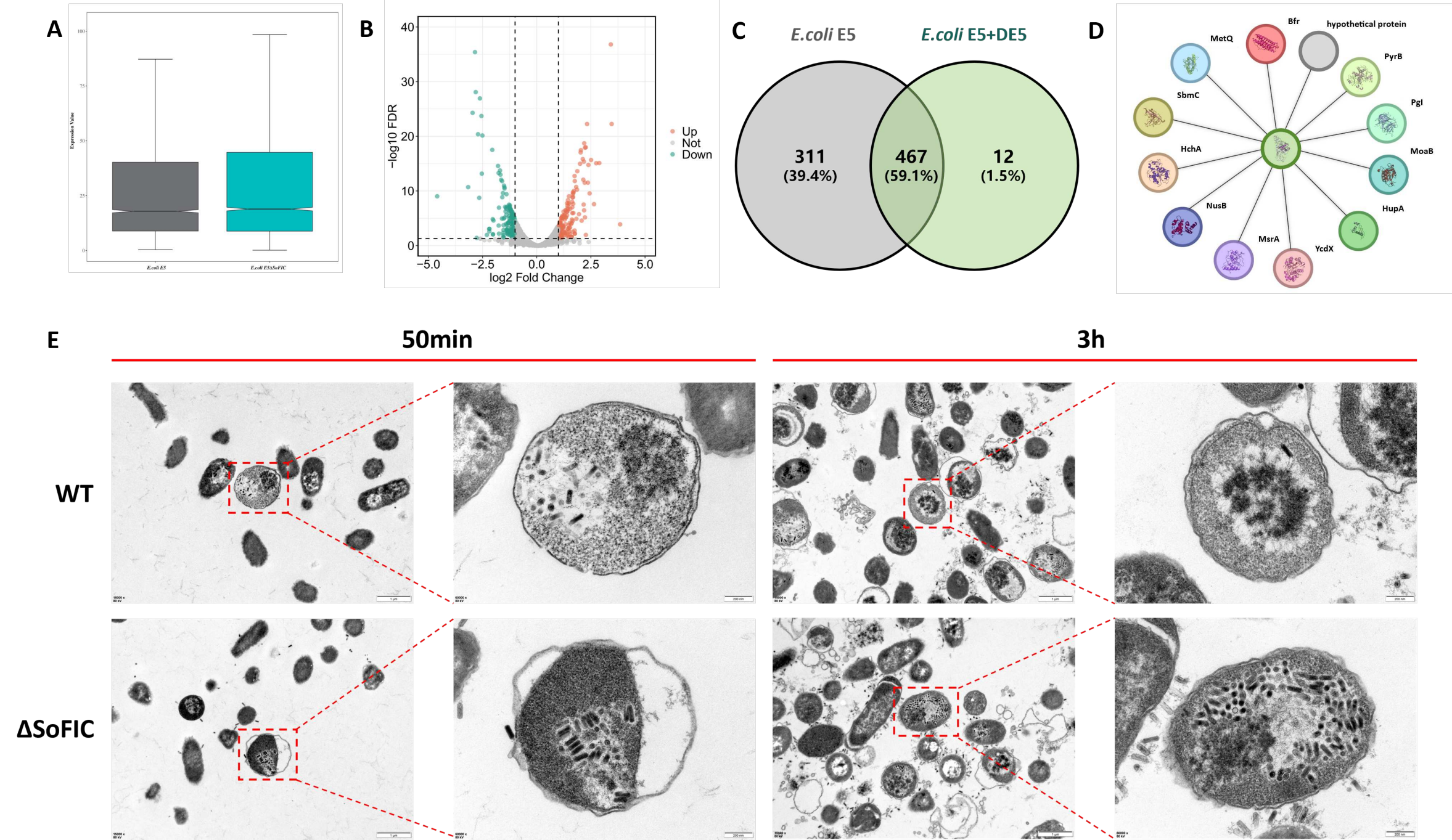
Escherichia coli E5

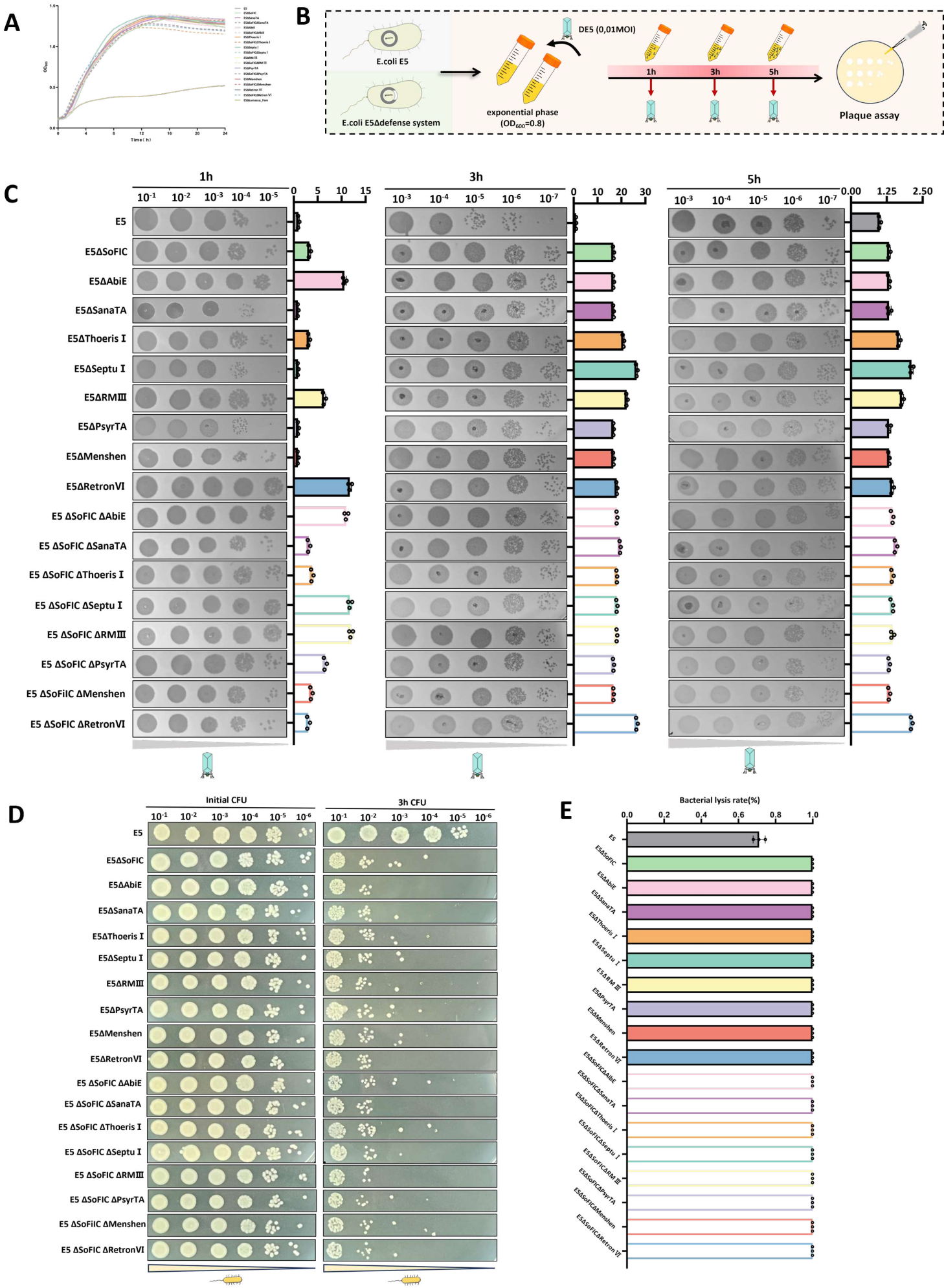
Fic motif: HPF[P/R]DGNGR


A
Escherichia coli E5
pET-28a
T7 promotor
177
281
Fic
sofic
B
T5
10-0 10-1 10-2 10-3 10-4 10-5
vector
SoFIC
SoFIC (H264A)
SoFIC (D268A)
SoFIC (R272A)
SoFIC(H264A/D268A/R272A)
C
T7
10-1 10-2 10-3 10-4 10-5 10-6
vector
SoFIC
SoFIC(H264A/D268A/R272A)
D
vB_EcoM_PD205
10-0 10-1 10-2 10-3 10-4 10-5
vector
SoFIC
SoFIC(H264A/D268A/R272A)
E
PFU/mL
T5
T7
vB_EcoM_PD205
vector
SoFIC
H264A/D268A/R272A
F
MOI=0.01
MOI=1
OD600
Time (h)
Vector
SoFIC
Vector+T5
SoFIC+T5


A
Phage titer[lg (PFU/ml)]
Time (min)
latent phase
rise phase
plateau
B
0.001MOI
0.01MOI
1MOI
10MOI
1h
3h
5h
E5
E5ΔSoFIC
E5ΔSoFIC-WT
E5ΔSoFIC-H264A
E5ΔSoFIC-D268A
E5ΔSoFIC-R272A
E5ΔSoFIC-H264A/D268A/R272A
C
0.001MOI
0.01MOI
1MOI
OD600
Time (h)
D
Initial CFU
3h CFU
E
Bacterial lysis rate(%)


A
OD600
Time（h）
E5
E5ΔSoFIC
E5ΔSoFIC-WT
E5ΔSoFIC-H264A
E5ΔSoFIC-D268A
E5ΔSoFIC-R272A
E5ΔSoFIC-H264A/D268A/R272A
C
Type I fimbriae
Curli fimbriae
P fimbriae
S fimbriae
ECP fimbriae
log2（RPKM+1）
log2(FC)
E.coli E5
E.coli E5ΔSoFIC
log2 FC
D
log2(Protein Intensity)
log2(FC)
E
log2 Fold Change
log2 (Protein Intensity)
UP
Not
Down
CsgG
CsgD
FimB
B
WT
ΔSoFIC
ΔSoFIC-WT
ΔSoFIC-3Mut
F
37℃
4℃
Adsorption efficiency(%)
Time（min）
G
DE5
E5
E5ΔSoFIC
E5ΔWaaL
BL21
H
O50
O2


A
Expression Value
E.coli E5
E.coli E5ΔSoFIC
B
−log10 FDR
log2 Fold Change
Up
Not
Down
C
E.coli E5
E.coli E5+DE5
311
(39.4%)
467
(59.1%)
12
(1.5%)
D
Bfr
hypothetical protein
MetQ
PyrB
SbmC
Pgl
HchA
MoaB
NusB
HupA
MsrA
YcdX
E
50min
3h
WT
ΔSoFIC


A
Time (h)
B
E.coli E5
E.coli E5Δdefense system
DE5 (0,01MOI)
exponential phase
(OD600=0.8)
1h
3h
5h
Plaque assay
C
1h
3h
5h
E5
E5ΔSoFIC
E5ΔAbiE
E5ΔSanaTA
E5ΔThoeris I
E5ΔSeptu I
E5ΔRMIII
E5ΔPsyrTA
E5ΔMenshen
E5ΔRetronVI
E5 ΔSoFIC ΔAbiE
E5 ΔSoFIC ΔSanaTA
E5 ΔSoFIC ΔThoeris I
E5 ΔSoFIC ΔSeptu I
E5 ΔSoFIC ΔRMIII
E5 ΔSoFIC ΔPsyrTA
E5 ΔSoFiIC ΔMenshen
E5 ΔSoFIC ΔRetronVI
D
Initial CFU
3h CFU
E
Bacterial lysis rate(%)

E.coli E5

E.coli E5ΔSoFIC

Biofilm

Curli fimbriae

Type Ⅰ fimbriae

fim gene cluster

csg gene cluster

Normal transcription

Fic

O-antigen （O2/O50）

DE5

Δ

FimB

CsgD

CsgG

HupA, SbmC

HR

NusB, PyrB, Bfr, MsrA

Metabolic collapse

Phage factory

RetronVI RMIII PsyrTA SoFIC Septu I

RetronVI RMIII PsyrTA SoFIC Septu I

Supplementary Files

This is a list of supplementary files associated with this preprint. Click to download.

- TableS1.xlsx
- Supplementarymaterial.docx